Graduate School ETD Form 9
(Revised 12/07)

PURDUE UNIVERSITY
GRADUATE SCHOOL
Thesis/Dissertation Acceptance

This is to certify that the thesis/dissertation prepared

By Renae Nelson

Entitled
Exploring the Mechanism of Action of Spore Photoproduct Lyase

For the degree of Master of Science

Is approved by the final examining committee:

Dr. Lei Li
Chair

Dr. Eric Long

Dr. Michael McLeish

To the best of my knowledge and as understood by the student in the *Research Integrity and Copyright Disclaimer (Graduate School Form 20)*, this thesis/dissertation adheres to the provisions of Purdue University's "Policy on Integrity in Research" and the use of copyrighted material.

Approved by Major Professor(s): Dr. Lei Li

Approved by: Dr. Eric Long 11/20/2013
Head of the Graduate Program Date

EXPLORING THE MECHANISM OF ACTION OF SPORE PHOTOPRODUCT LYASE

A Thesis

Submitted to the Faculty

of

Purdue University

by

Renae Nelson

In Partial Fulfillment of the

Requirements for the Degree

of

Master of Science

December 2013

Purdue University

Indianapolis, Indiana

To Steven, thank you for holding my hand as we've grown up together. To my children, Adelene and Calvin, thank you for motivating me to be the best person I can be. To my Momma, for making me think that a master's degree made you the smartest person in the world.

ACKNOWLEDGEMENTS

I would like to thank Dr. Lei Li for providing me with the opportunity to challenge and develop my skills as a research scientist, and his constant patience with my failures as well as my successes. I would also like to express my appreciation to LinLin Yang for patiently teaching me and molding my knowledge of biochemistry and experimental methodology. To the members of Dr. Li's laboratory; Gengjie Lin, Yajun Jian, and David Ames, thank you for your support and guidance. The research contained herein was a collaborative effort, and would not have been possible without your diligent work. I would also like to thank Dr. Long, for helping me realize the real reward of hard work. Thank you, Dr. McLeish, for your honest perspectives and for always challenging me. To Karl Dria, thank you for the many hours you spent training me on the QTOF.

TABLE OF CONTENTS

Page

Page

LIST OF TABLES

Table Page

LIST OF FIGURES

Figure Page

LIST OF ABBREVIATIONS

SPL	spore photoproduct lyase
SP	5-thyminyl-5,6-dihydrothymine, also called spore photoproduct
SAM	S-adenosylmethionine
5'-dA•	*5'*-deoxyadenosyl radical
Py	pyridine
Ac	acetyl
TFA	trifluoroacetic acid
ACN	acetonitrile
DMF	dimethylformamide
HOAc	acetic acid
TLC	thin layer chromatography
HPLC	high performance liquid chromatography
EPR	electron paramagnetic resonance
MS	mass spectroscopy
ESI	electrospray ionization
QTOF	quadrupole time-of-flight
SDS-PAGE	sodium dodecyl sulfate polyacrylamide gel electrophoresis

ABSTRACT

Nelson, Renae. M.S., Purdue University, December 2013. Exploring the Mechanism of Action of Spore Photoproduct Lyase. Major Professor: Lei Li.

Spore photoproduct lyase (SPL) is a radical SAM (S-adenosylmethionine) enzyme that is responsible for the repair of the DNA UV damage product 5-thyminyl-5,6-dihydrothymine (also called spore photoproduct, SP) in the early germination phase of bacterial endospores. SPL initiates the SP repair process using *5'*-dA• (*5'*-deoxyadenosyl radical) generated by SAM cleavage to abstract the H_{6proR} atom which results in a thymine allylic radical. These studies provide strong evidence that the TpT radical likely receives an H atom from an intrinsic H atom donor, C141 in *B. subtilis* SPL. I have shown that C141 can be alkylated in native SPL by iodoacetamide treatment indicating that it is accessible to the TpT radical. Activity studies demonstrate a 3-fold slower repair rate of SP by C141A which produces $TpTSO_2^-$ and TpT simultaneously with no lag phase observed for $TpTSO_2^-$ formation. Additionally, formation of both products shows a $^{D}V_{max}$ kinetic isotope effect (KIE) of 1.7 ± 0.2 which is smaller than the $^{D}V_{max}$ KIE of 2.8 ± 0.3 for the WT SPL reaction. Removal of the intrinsic H atom donor by this single mutation disrupts the rate-limiting process in the enzyme catalysis. Moreover, C141A exhibits ~0.4 turnover compared to the > 5 turnovers in the WT SPL reaction.

In Y97 and Y99 studies, structural and biochemical data suggest that these two tyrosine residues are also crucial in enzyme catalysis. It is suggested that Y99 in *B. subtilis* SPL uses a novel hydrogen atom transfer pathway utilizing a pair of cysteine-tyrosine residues to regenerate SAM. The second tyrosine, Y97, structurally assists in SAM binding and may also contribute to SAM regeneration by interacting with radical intermediates to lower the energy barrier for the second H-abstraction step.

CHAPTER 1. BACKGROUND

1.1 Introduction: Spore Photoproduct Lyase

Spore photoproduct lyase (SPL) is a radical SAM enzyme expressed in germinating *Bacillus subtilis* endospores that efficiently repairs the unique thymine dimer 5-thyminyl-5,6-dihydrothymine, commonly referred to as spore photoproduct (SP). The formation of SP is a direct result of UV damage to DNA in dormant endospores. Following a background discussion on endospores and SP, this thesis will closely examine SPL; beginning with previous research in the field and culminating in the contribution of my research to the currently proposed mechanism of action of this critical DNA repair enzyme.

1.2 Bacterial Endospores

Bacterial endospores are the cause of numerous health afflictions to humans. For example: anthrax caused by *Bacillus anthracis*, botulism from *Clostridium botulinum*, gas gangrene from *Clostridium perfingens*, and tetanus caused by *Clostridium tetani* (1). The harmful nature of these diseases demands a greater understanding of these endospores and the resistance they exhibit to standard sterilization means. The lifecycle of spore-forming bacteria *B. subtilis* is depicted in Figure 1.1 (2). During times

when nutrients are plentiful and conditions are favorable, the cell undergoes vegetative cycle of metabolically active growth and cell division. However, when under stress, bacteria produce an endospore which allows them to withstand difficult conditions such as exposure to high temperatures, starvation, extremes in pH, chemical damage, enzymatic destruction and UV irradiation (4,7).

Endospore formation is most prevalent in Gram-positive bacteria such as *B. subtilis.* Our focus will be on this bacteria and specifically the innate resistance of *B. subtilis* to UV irradiation, as it is most pertinent to this body of research.

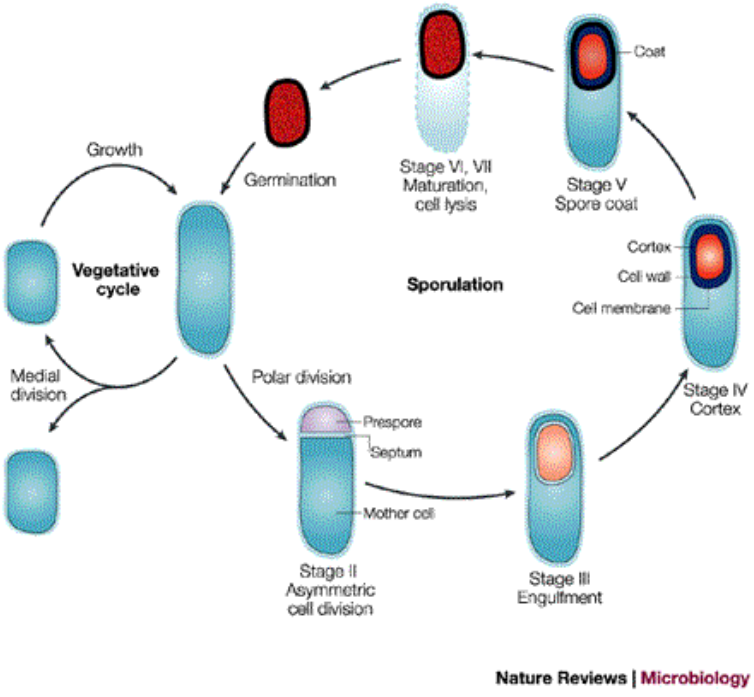

Figure 1.1: Endospore Formation in *Bacillus Subtilis* (2)

Vegetative cells undergo the differentiation cycle, sporulation, in the formation of endospores (Figure 1.1) (2). During sporulation, the bacterium's DNA is replicated and a forespore (prespore) is created, which serves as the central core of the endospore, shown as Stage II. The forespore is then enveloped by the mother cell (Stage III) and by intercellular communication, endospore-specific compounds are synthesized to form the cortex, cell wall, cell membrane and spore coat in Stages IV and V (7). All of which protect the integrity of the spore and its hereditary material (4). Final maturation concludes in Stage VI and VII with dehydration of the endospore and lysis of the mother cell, releasing a dormant endospore (7). The transitions through each of the stages of endospore formation are coordinated by sigma factors which are small proteins that initiate specific gene expression by directing RNA polymerase to specific sites on DNA (7). The resulting endospore (Figure 1.2) (3) is protected from destruction and is able to survive in this stage for great lengths of time. Once environmental conditions become favorable, the endospore will move into the germination stage and carry on with its lifecycle.

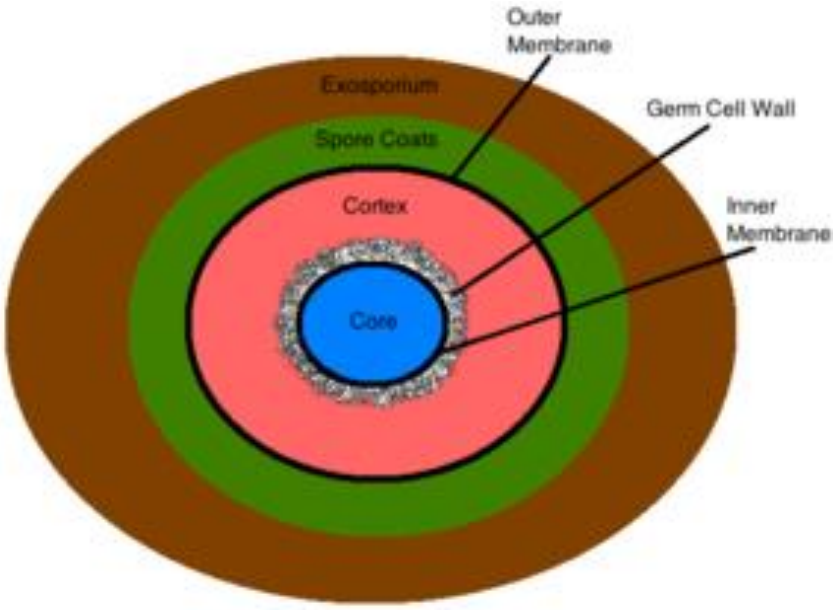

Figure 1.2: Structure of Endospore (3)

The structure and chemical composition of the endospore is critical to its survival. Externally, the spore coat provides the first line of defense against physical and chemical disruption. It is comprised of an electron-dense outer coat and an electron-translucent inner coat. Several proteins of the spore coat have been isolated and characterized, including; CotX and CotY, which appear to be cross-linked either by disulfide, *o,o*-dityrosine bonds or both (5). This cross-linking provides a strong defense against lytic enzymes. The spore coat also has the ability to counteract chemical agents. The cortex which lies beneath the coat is composed of specialized peptidoglycan that is necessary for dehydration of the spore core (7). The spore coat and cortex of the endospore provide resistance and dormancy. Additionally, they are essential in the response system when molecules that trigger germination are present (8). Further resistance of

the endospore to destruction via external forces (lytic enzymes, wet/dry heat) can be attributed to: the engulfing glycoprotein layer known as the exosporium which allows the endospore to withstand extreme temperatures, an inner membrane that has low permeability which blocks many chemicals from entering the core, and the lower water content in the core which also protects against wet-heat (8). The core contains the genomic DNA, ribosomes and up to 10% of the spore's dry weight in dipicolinic acid. Dipicolinic acid is specific to endospores and is believed to play a role in spore dormancy and heat resistance (7).

Internally, the endospore provides resistance (specifically to UV irradiation which leads to the formation of spore product, SP) in two ways; genomic DNA is surrounded with small acid-soluble proteins (SASPs) that tightly bind to and condense the DNA, restricting access; and a specific DNA repair process that is efficiently utilized when damage has occurred (4). These protections afforded the dormant bacteria while in endospore form which protect against UV damage are of particular interest to our research group. Further discussion on this topic will include: structure of DNA in endospores, formation of UV damage products and function of surrounding SASPs; as well as detailed discussion on the repair system utilized by the endospores to repair any accumulated UV induced DNA damage prior to germination.

1.3 Structure of Genomic DNA

UV irradiation is a standard means for sterilization of many bacteria. Endospores, however, have acquired resistance to UV irradiation. This can be partially attributed to

the conformation of genomic DNA and the surrounding proteins that protect the DNA, direct the UV damage that does occur, and repair any resulting damage.

Spore genomic DNA is complexed with α/β-type small acid-soluble proteins (SASPs) (9). The function of these proteins is to provide a protective barrier by tightly binding and condensing the DNA. During sporulation transcription is activated via sigma factors in the formation of the forespore which expresses the *sspA* and *sspB* genes encoding SASP-α, and SASP-β in *B. subtilis* (22). The α/β-type SASPs have a highly conserved region of 59-72 residues in *Bacillus* species. *In vitro* studies have shown the following interactions of the SASPs complexed with DNA: (i) double-stranded DNA is the only form bound, (ii) most tightly bound are the GC-rich regions of DNA, (iii) lowering the pH (under 7) increases the affinity of α/β-type SASPs for DNA, (iv) every four base pairs contains one α/β-type SASPs, and (v) cooperative binding is observed between the DNA and α/β-type SASPS (9).

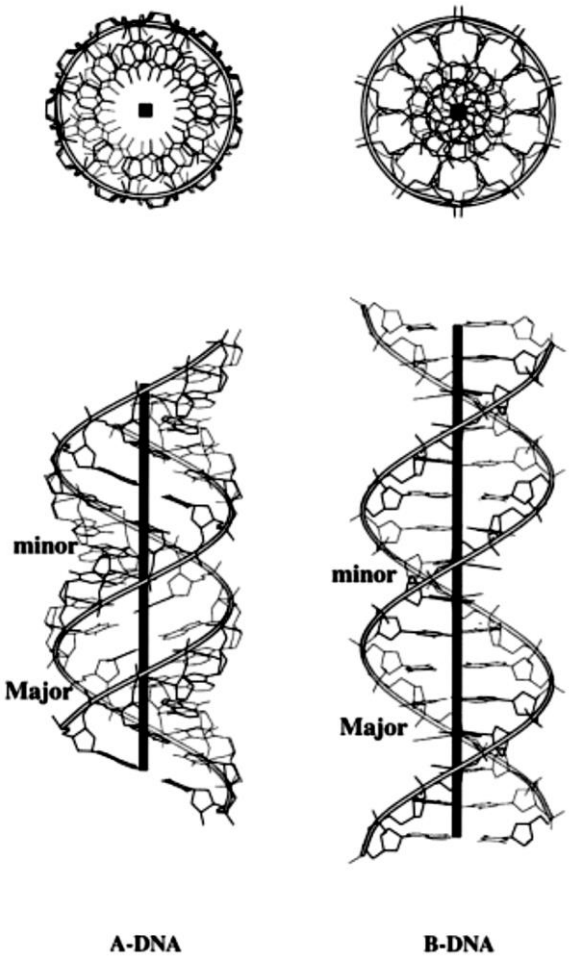

Figure 1.3: A and B Form DNA (6) (Adapted With Permission)

DNA can occur in different three-dimensional forms. It is comprised of nucleotides containing a nitrogenous base (adenine, guanine, cytosine, or thymine), a *2'*-deoxy-ribose, and a phosphate. There is a great deal of flexibility in the bonds of the phosphodeoxyribose backbone which allows for stretching, bending and unpairing of the strands of DNA (11). Variations in the structure of DNA are due to different conformations of the deoxyribose, as well as rotation in the bonds of the backbone. There are two primary forms that exist in cellular DNA: 1) B-form (Watson-Crick

structure) which is the most stable under physiological conditions, and 2) A-form which is most prevalent under conditions of low water content. B-form DNA has a diameter of ~20 Å, 10.5 base pairs per helical turn and displays a 3.4 Å rise in the helix per base pair. On the other hand A-form DNA is ~26 Å in diameter, 11 base pairs per turn with a rise of 2.6 Å between the base pairs (11). This indicates that in the absence of water the DNA is very compact, less accessible for external interaction and has a more restricted freedom of rotation when compared to B-form DNA.

When bound, the effect of SASPs on the structure of DNA and other proteins in the complex is significant. In addition to the dehydration of the spore core, the SASP/DNA complex binding induces a DNA helical conformation from B-form to A-form (Figure 1.3) (6,14). This conformational change dramatically affects the possible UV-induced DNA damage products that may form.

1.4 UV-Induced DNA Damage Products

DNA contains four nitrogenous bases: adenine (A), cytosine (C), thymine (T) and guanine (G). Of these, thymine (T) is most sensitive to UV damage (10,12). Density functional theory (DFT) studies have shown that the sensitivity displayed by thymine can be explained by; a more favorable reaction energy for thymine photodimerization compared to that of cytosine dimers or cytosine-thymine dimers (10). This can be attributed to a comparatively high S_1 energy state of the thymine reactant complex combined with the fact that the ground-state transition structure (at the nuclear configuration) displays an absolute minimum in the excited-state energy curve in the

thymine dimer system (9.2 kcal/mol below S_1 state for T-T vs. 6.9 kcal/mol above S_1 for C-C) (10). Lastly, it was determined that T-T system ground-state transition structure displays the smallest S_2-S_0 energy gap and the most favorable excited-state energy barriers, making thymines more sensitive to UV-induced pyrimidine dimer formation than cytosine (10).

Typically, the genomic DNA of cells adopts a B-conformation (Figure 1.3), which, when exposed to UV irradiation leads to the formation of cyclobutane pyrimidine dimer (CPD) and pyrimidine (*6-4*) photoproduct as the most common UV damage products (Figure 1.4) (10).

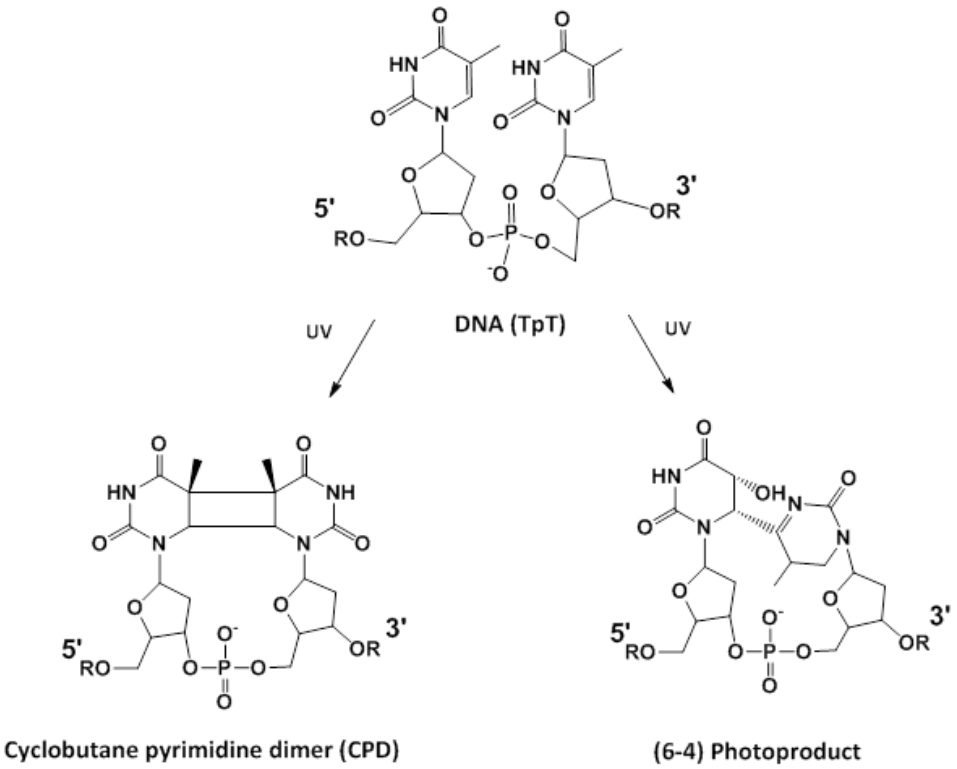

Figure 1.4: UV Induced DNA Damage Products

Cyclobutane pyrimidine dimers (CPDs) form by covalent linkage between C_6 and C_5 of adjacent thymines. As shown in Figure 1.4, the resultant structure contains a four membered ring. Research has shown that in nucleosome core DNA of bacterial cells in the vegetative state, the frequency of CPDs occurs every 10.3 (+/-0.1) base pairs (34). Formation of 6-4 photoproduct, on the other hand, is more random throughout the nucleosome core domain with 1/3 the frequency of CPDs (35). Both of these UV damage products may be repaired either by nucleotide excision repair (NER) in which the dimer is excised from the single strand DNA and repaired by DNA polymerase and DNA ligase, or by photoreactivation whereby DNA photolyase is activated by absorption of a photon and transfers an electron to the damage site (36).

However, in endospores the genomic DNA is in the A-conformation (Figure 1.3) due to low water content and the small acid-soluble proteins (SASPs) which bind the DNA (9, 14). This A-conformation of the complexed DNA yields a unique thymine dimer, 5-thyminyl-5,6-dihydrothymine (commonly referred to as spore photoproduct or SP) as the primary DNA UV damage product (Figure 1.5).

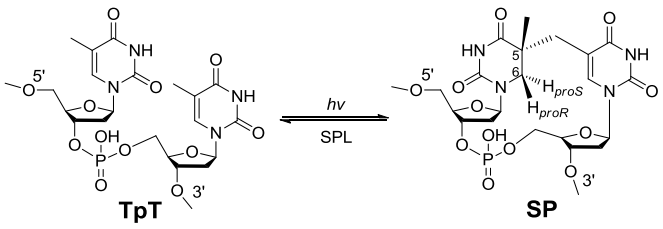

Figure 1.5: Spore Photoproduct (SP) (20)

When exposed to 254 nm UV light, 95% of the total photoproducts in the genomic DNA of endospores were shown to be SP and only 5% existed as cis-syn cyclobutane pyrimidine dimers (16). Additionally, as many as 8% of the total thymine residues in genomic DNA were found to be in the form of SP following UV irradiation (17,18).

1.5 Formation of SP

In the formation of SP, a chiral center is created at carbon C_5 which may exist in either an *R* or *S* configuration and depends upon whether the dinucleotide is *5'→3'* or *3'→5'* as shown in Figure 1.6. By irradiating unmodified thymine-thymine dinucleoside monophosphate, researchers produced SP TpT that was further characterized via HPLC and NMR (19). They concluded that the SP TpT formed was dinucleotide *5'→3'* with an *R* configuration at carbon C_5. (19). In double-stranded DNA, thymine radical reactions with adjacent nucleosides are more likely when thymine is on the *3'*-end. This is due to a shorter distance between the adjacent *5'*-end and the C_5, C_6, or methyl group of the thymine moiety (In A-form DNA: C-C distances between $Me_{3'}$ and $C_{5'}$ = 3.69 Å and between $Me_{5'}$ and $C_{3'}$ = 5.52 Å) (19).

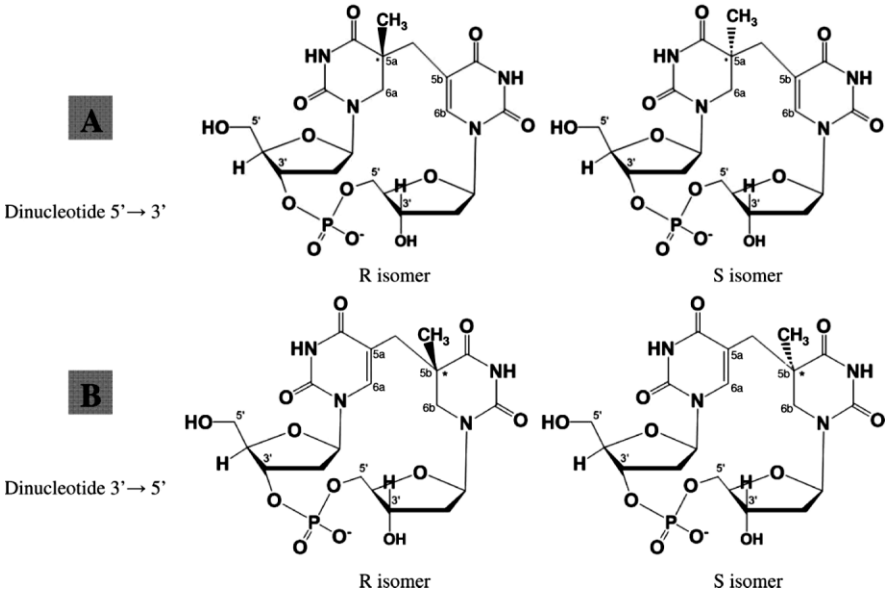

Figure 1.6: Formation of SP Isomers (19)

Building upon previous work in which the absolute configuration of the C_5 was determined to be *R,* researchers in Dr. Li's laboratory performed additional deuterium labeling studies of dinucleotide TpT. They determined that SP photoformation occurs through an intramolecular H atom transfer process between two thymine residues (20, 21).

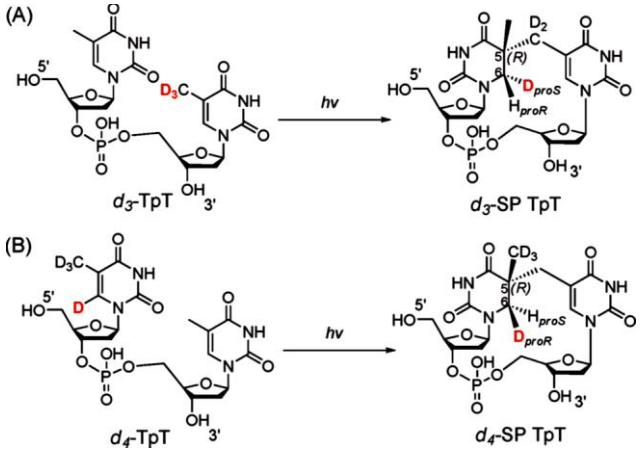

Figure 1.7: Deuterated SP Derivatives (20)

Under the assumption that during the photochemical formation of SP, one of the H atoms from the original *5'* –thymine (*5'*-T) residues remains and the other comes from the *3'*-T methyl group, deuterium labeled TpT dinucleotides were prepared. Figure 1.7 demonstrates the d_3- TpT and d_4- TpT that were selectively synthesized to explore this H atom transfer (20). Analysis by ^{1}H NMR spectroscopy allowed for the monitoring of the hydrogen-/deuterium-atom transfer process. It was determined that a hydrogen atom from the methyl group of *3'* thymine (*3'*-T) is transferred to the $C_{6pro\text{-}S}$ atom of *5'*-T intramolecularly and diastereoselectively. These findings led to the following proposed mechanism for the SP photoreaction (Figure 1.8) (21). Following UV exposure, the C=C of the *5'*-T forms a pair of radicals. The $C_{6pro\text{-}S}$ then abstracts an H-atom from the *3'*-T methyl group leading to the formation of a 5-α-thyminyl and 5,6-dihydrothymin-5-yl radical. These two radicals then recombine yielding the final SP product.

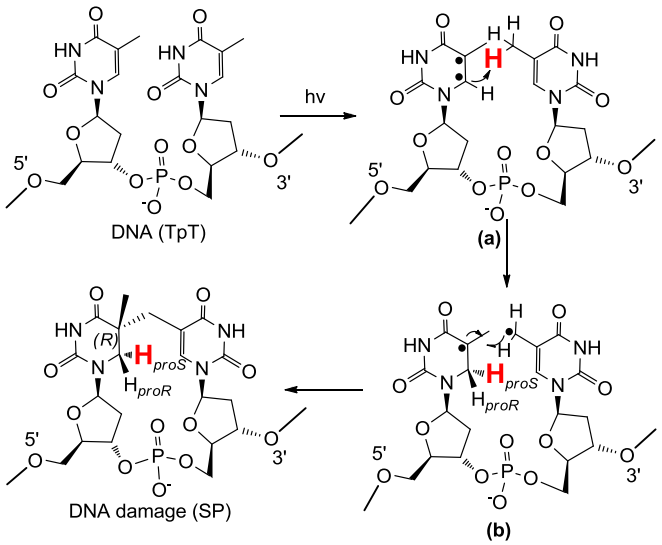

Figure 1.8: Proposed Mechanism of SP Formation (20)

Having a better understanding of the mechanism of SP formation, we will now take a look at the DNA repair pathways available to endospores to repair accumulated UV damage in the early germination phase.

1.6 UV-Induced DNA Damage Repair Pathways

In addition to the protection afforded endospore genomic DNA by its conformation and associated SASPs, which reduce the formation of all but one UV damage product (SP), the resulting DNA damage product (SP) are efficiently repaired during the early germination phase. In trying to penetrate these defense mechanisms of the endospore against UV damage, we take an in-depth look at one area of weakness in these defenses: the repair mechanisms for SP. SP accumulates in endospores during the dormant phase and is efficiently repaired in the early stage of germination (20,21).

The accumulation of SP is due to the fact that during dormancy the spores are metabolically inactive (22). In order to reactivate and return to vegetative growth, the resultant DNA damage must be repaired. During the phases (vegetative, sporulation and germination) of the endospore, there are two pathways which can be involved in DNA repair. The first is the nucleotide excision repair (NER) pathway mediated by the *uvr* excinuclease genes which are expressed as three subunits (*uvrABC)* in *B. subtilis* (22). In this pathway, the SP is excised and the resulting single-stranded gap is filled by DNA polymerase and DNA ligase.

The second repair pathway is through the *in situ* monomerization of SP into two thymine residues initiated by spore photoproduct lyase (SPL) (23). During spore

formation, transcription is initiated by σ-G RNA polymerase for the expression of *splB*, the gene that encodes SPL (22). SPL is then packaged and stored in the dormant spore until activated in the early germination phase.

These two pathways (NER, SPL) are closely regulated at the transcriptional level. Research by Meoller *et.al*. (22) showed that in response to DNA damage during vegetative growth and germination, LexA/RecA mediates the NER pathway, although this is not seen during sporulation. Rather, the transcription of *splB* is not induced by DNA damage, nor is it observed during vegetative growth or germination but only during the sporulation phase (22).

1.7 Spore Photoproduct Lyase (SPL)

This discussion of SPL, specifically from *Bacillus subtilis* strain 168 (which is the strain used in subsequent research studies in this thesis), will include: (i) background on the radical SAM enzyme family to which SPL belongs; and (ii) the proposed mechanism of action prior to the body of research outlined herein.

1.7.1 Radical SAM (S-adenosylmethionine) Superfamily of Enzymes

In exploring the mechanism of action of SPL, it is critical to understand the role of cofactors involved in the enzyme repair process. Two components necessary to initiate the repair of SP TpT are SAM (S-adenosylmethionine) and a 4Fe-4S cluster (Figure 1.9).

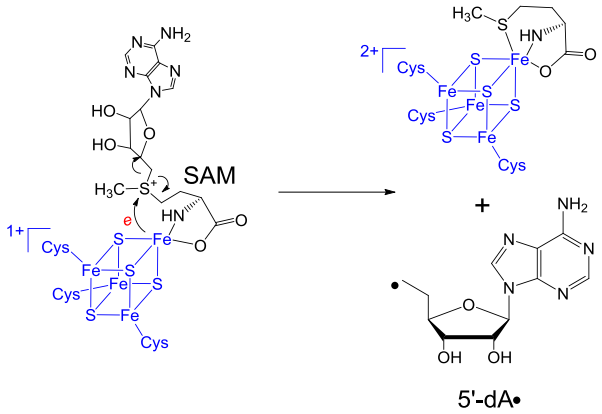

Figure 1.9: SAM Reductive Cleavage with Electron Provided by the [4Fe-4S]$^{+}$ Cluster to Yield the *5'*-dA• and Methionine in Radical SAM Enzymes (23).

SPL belongs to the radical SAM (S-adenosylmethionine) superfamily of enzymes. This family is characterized by a CXXXCXXC motif. The three cysteine residues are ligands for three irons in a [4Fe-4S] cluster, with the fourth iron coordinated by SAM in a bi-dentate manner. The fourth and fifth ligands to the cluster come from the amino and carboxylate moieties of SAM (21,23). In the +1 oxidation state, the cluster donates an electron to SAM, reductively cleaving its C-S bond, and generating a *5'*-dA• which catalyzes SP repair via a radical mechanism (Figure 1.10).

1.7.2 Previously Proposed Mechanism of SPL

Early *in vivo* studies by Donnellan and Stafford (1968) suggested that in the absence of light, SP was repaired in germinating spores via a direct reversal strategy (17). Tritium labeled thymine was exposed to UV irradiation to generate SPs which were not found to leak tritium into the media following SP repair. Should the mechanism of repairing this DNA damage include excision of the thymine dimer, the tritium labeled

thymines should be found in the media, which was not the observed (17). Further studies conducted by Wang *et.al*. (28) proved that the disappearance of radioactivity from SP seemed to occur stoichiometrically with that of appearance in thymine, which further supported the direct-reversal repair hypothesis (28).

Later, it was determined that SPL was an iron-sulfur enzyme (29) that also employed SAM cleavage (to *5'*-dA•) to catalyze the SP repair process (30). The repair process of an SP analogue was determined to be initiated by abstraction of a hydrogen atom at the C_6 position. This hydrogen atom abstraction reaction could have been regulated by the SAM cleavage reaction which produces the *5'*-dA• (31).

More recently, tritium-labeling of thymine residues showed recovery of tritium-labeled SAM following the SPL reaction. Regeneration of SAM following each catalytic turnover was suggested due to the necessity for only one SAM molecule to catalyze > 500 turnovers (32). Germinating spores may have limited amounts of SAM which lead to the possibility of regeneration and reuse of this cofactor (Figure 1.10), however the mechanism of SAM regeneration following SPL catalysis had yet to be established. The research conducted here aims to shed light on this process (Chapter 3).

The hypothesized direct-reversal repair reaction mechanism is shown in Figure 1.10. Initiation of this process begins with a SAM cleavage reaction in which the generated *5'*-dA• abstracts an H atom from the C_6 position of SP. This is followed by β scission of the methylene linkage between the two thymines. As proposed, the thyminyl radical is then quenched by an H-atom back transfer from the *5'*-dA resulting in the repaired thymine dimer.

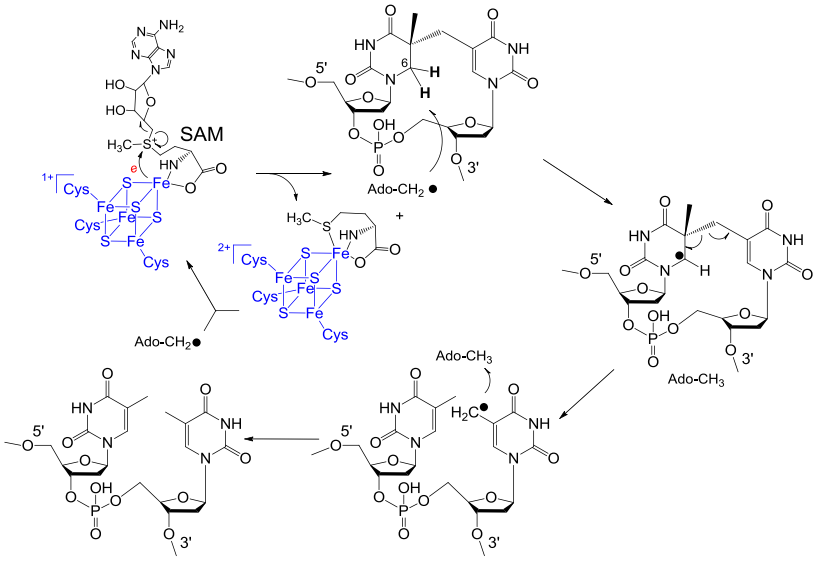

Figure 1.10: Proposed Mechanism of SP Repair Using SAM (23)

Initially, theoretical calculations challenged this mechanism (37,38). If indeed the *5'*-dA is involved in both the H atom abstraction at the *5'*-T of SP and the H atom back donation to the methyl radical at the *3'*-T, it has to shift down one nucleotide (approximately 3.4 Å under the then assumed B-form DNA) to complete this repair. However, this shift is not only energetically unfavorable but would require a significant conformational change in the protein. Calculations predicted that an additional H atom exchange step must exist between the two methyl groups of the thymine to return the radical to the *5'*-T prior to the H atom back donation step between the *5'*-dA and the thymine radical. Should a protein residue be involved in this H atom transfer process, this intermediate H atom exchange step would be unnecessary (38).

1.8 Research Goals

The research presented in this thesis was guided by two primary goals in the exploration of the mechanism of action of SPL. The first objective was to confirm the identity of the intrinsic H-atom donor to the thymine allylic radical generated by *5'*-dA• in the initiation of the SP repair process. C141 has long been proposed to be this donor but the exact role of this residue in the H atom donation was not fully understood. The research presented here provides conclusive evidence to confirm these previous assumptions. In the journal article "Mechanistic Studies of the Spore Photoproduct Lyase via a Single Cysteine Mutation" published in *Biochemistry* in 2012 (41), the role of C141 in the enzymatic catalysis of SPL is explored. Chapter 2 of this thesis will provide a more in depth discussion on the research conducted and the conclusions drawn from these studies which identify C141 as the likely H donor to the thymine allylic radical generated by *5'*-dA• in the initiation of the SP repair process.

The second objective of this work was to explore the binding and regeneration of SAM in the mechanism of SPL. These studies have identified the role of two conserved tyrosines (Y97, Y99 in *B. subtilis*) that are essential in this enzymatic catalysis. It is believed that Y99 participates in a novel hydrogen atom transfer (HAT) pathway to regenerate SAM, while Y97 aids in a structural capacity to facilitate SAM binding as well as contributing to SAM regeneration. "A Radical Transfer Pathway in Spore Photoproduct Lyase" published in *Biochemistry* in 2013 (42), takes a closer look at the two tyrosine residues, Y97 and Y99 in *B. subtilis* SPL, which are believed to aid in the

repair pathway by regenerating SAM for subsequent enzymatic turnovers. Further discussion of this radical transfer pathway follows in Chapter 3.

CHAPTER 2. "MECHANISTIC STUDIES OF THE SPORE PHOTOPRODUCT LYASE (SPL) VIA A SINGLE CYSTEINE MUTATION"

2.1 Introduction

Spore photoproduct lyase (SPL) repairs the UV damage product 5-thyminyl-5,6-dihydrothymine, or spore photoproduct (SP). SP is the exclusive DNA photo-damage product in bacterial endospores. The proposed mechanism of repair demonstrates that SPL employs the *5'*-dA• generated by cleavage of SAM to abstract the H_{6proR} atom of SP leading to a thymine allylic radical which then takes an H atom from a source believed to be cysteine 141 of SPL from *B. subtilis*.

Experimental evidence supporting the involvement of a protein residue in the repair process was provided by *in vivo* mutation studies by Nicholson and coworkers (39). There are four conserved cysteine residues in *B. subtilis* SPL; C91, C95, C98, and C141. The radical SAM CX_3CX_2C motif contains the first three cysteines which if mutated would destabilize the [4Fe-4S] cluster and render the enzyme inactive. Research showed that mutation of C141 equally disrupted enzymatic activity of SPL, suggesting that this protein residue must play some role in the repair process (39).

Further proof was provided by the studies of Fontecave (40) which demonstrated that the H-atom back donation step was interrupted by the C141A mutation. *In vitro* studies utilizing dinucleotide SP TpT under reducing conditions (excess sodium dithionite) produced a $TpTSO_2^-$ species as the major product following repair by SPL C141A. The $\bullet SO_2$ group, originating from the hemolytic cleavage of the S-S bond in dithionite, was attached to the methyl group of the *3'*-T as illustrated in Figure 2.1. This suggests that in the absence of C141, the radical on the methyl group of the *3'*-T is quenched by a moiety other than *5'*-dA as hypothesized in the initial reaction mechanism.

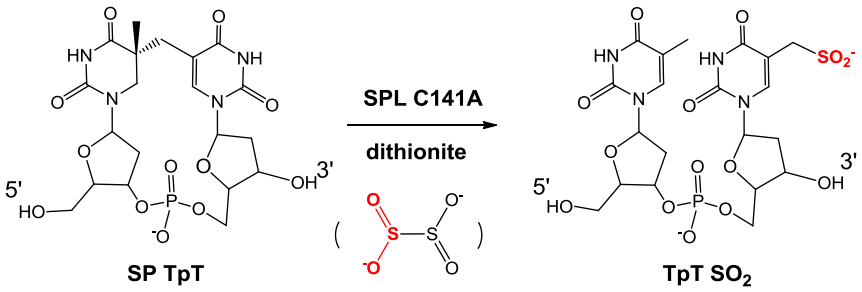

Figure 2.1: Formation of $TpTSO_2^-$ (41)

These findings led to a revised reaction mechanism for SPL catalyzed SP dimer repair, in which C141 is the proposed H atom donor in quenching the *3'*-T radical to restore TpT (Figure 2.2).

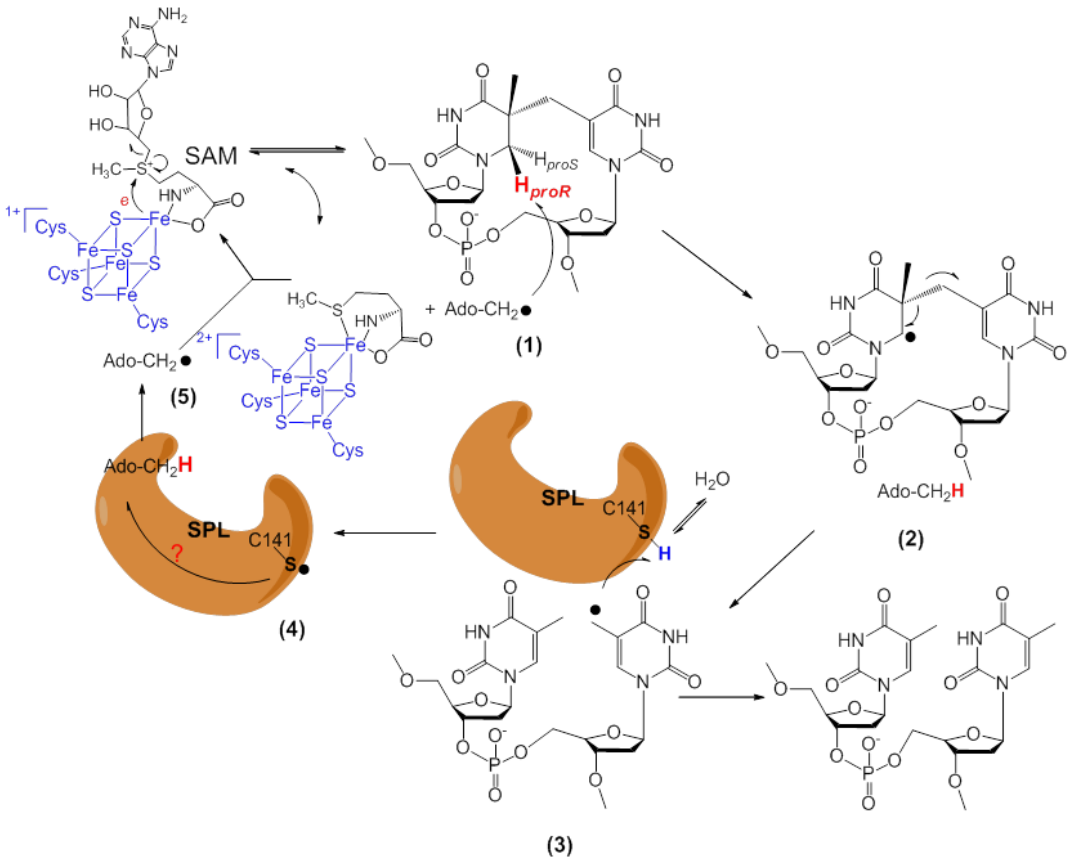

Figure 2.2: Updated Mechanism of SPL (41)

SPL uses the *5'*-dA• to abstract a H atom from SP, forming an SP radical that undergoes β scission to form a repaired *5'*-T and a *3'*-T allylic radical. Previous studies (20) have proposed that the TpT radical receives an H atom back from *5'*-dA•, however, it is now believed that this H atom comes from a protein residue which is able to utilize acid-base chemistry to exchange a proton with the aqueous solution to repair TpT. The research presented in this thesis confirms initial suggestions that this thymine allylic radical takes an H atom from cysteine 141 resulting in a putative thiyl radical (Figure 2.2). These new developments in the currently hypothesized mechanism of action of SPL will be further explored here.

To explore C141 as the intrinsic H atom donor, I performed the following assays: (1) Iodoacetamide labeling studies to prove the accessibility of C141A to the solvent and thus TpT; (2) Activity assays for C141A mutant SPL to monitor the effect of this mutation on the rate of repair of SP; (3) Product analysis to quantify the repair products following SPL catalysis; and (4) Isotope effect assays to identify the role of C141 in the closed catalytic cycle of SP repair by SPL.

2.2 Experimental Methods

2.2.1 Expression and Purification of SPL C141A Mutant

The protein purification as well as the enzyme reactions were carried out under an inert atmosphere using a Coylab anaerobic chamber (Grass Lake, MI) with the H_2 concentration around 3%. Both the WT SPL and the C141A mutant were expressed in LB (Luria Bertani) medium containing the antibiotics ampicillin (100 µg/mL) and kanamycin (25 µg/mL) as previously described (21). The proteins were purified via Ni-NTA chromatography followed by an ion exchange chromatography using the SP Sepharose fast flow ion exchange resin (GE Healthcare Life Sciences, Piscataway, NJ). The bound protein was washed using a buffer containing 25 mM Tris, 250 mM NaCl and 10% glycerol (pH 7.0) for 10 column volumes. The protein was then eluted using the same buffer containing 500 mM NaCl instead. The resulting protein was diluted by 2-fold to reduce the salt concentration to 250 mM and saved for activity studies. (41)

2.2.2 Protein, Iron and Sulfide Assays

Routine determinations of protein concentration were conducted by the Bradford method,(44) using bovine gamma globulin as the protein standard. Protein concentrations were calibrated on the basis of the absorption of aromatic residues at 280 nm in the presence of 6 M guanidine hydrochloride using the method of Gill and von Hippel using the value of 37460 for the molar absorptivity coefficient for SPL(45). Iron content was determined using *o*-bathophenanthroline (OBP) under reductive conditions after protein digestion in 0.8% $KMnO_4$ and 1.2 M HCl as described by Fish (46). Iron standards were prepared from commercially available ferric chloride. Sulfide assays were carried out using the method described by Beinert (47).

2.2.3 SPL C141A Activity Assay

In a typical set of experiments, the reaction mixture contained 30 µM SPL C141A, 0.6 mM SP TpT substrate, 100 µM SAM in buffer containing 25 mM Tris, 250 mM NaCl and 10% glycerol at pH 7.0 (total volume 500 µL). Freshly made sodium dithionite (final concentration 1 mM) was added as the reductant to initiate the enzyme reaction. The reaction was conducted as described before and analyzed by HPLC (21). In a separate set of experiments, the C141A mutant reaction was examined in phosphate buffer (containing 25 mM sodium phosphate instead of 25 mM Tris) to exclude the involvement of Tris in enzyme catalysis (41).

2.2.4 HPLC Assay for Product Analysis

HPLC Chromatography was performed at room temperature with a Waters (Milford, MA) breeze HPLC system with a 2489 UV/Visible detector at 268 nm. An Agilent Zorbax reverse-phase C-18 column (3.5 µM, 4.6×50 mm) was equilibrated in 50 mM triethylammonium acetate, pH 6.5 (buffer A), and compounds were eluted with an ascending gradient (5% – 20%) of buffer B (which is composed of 50% buffer A and 50% acetonitrile) at a flow rate of 1 mL/min for 15 minutes. Under this gradient, SP TpT was eluted at 5.4 min, 5'-dA at 8.9 min, $TpTSO_2^-$ at 9.8 min, TpTOH at 12.9 min and TpT at 14.1 min. The identity of the products was confirmed by co-injection of respective authentic samples as well as by LC-MS spectrometry. The area of the product peak was determined after subtraction of the baseline from the t = 0 chromatograph and the amounts of 5'-dA, $TpTSO_2^-$ and TpT formed were determined by reference to standard curves constructed with authentic samples (41).

2.2.5 LC-MS Assay for Product Analysis

LC-MS analyses were conducted via an Agilent 6130 Quadrupole LC/MS spectrometer coupled to an Agilent 1100 series chromatography system using a Waters X-bridge^{TM} OST C18 column (2.5 µM, 4.6×50 mm). The column was equilibrated in solvent A (5 mM ammonium acetate, pH 6.5), and compounds were eluted with an ascending gradient (0 – 17%) of solvent B (5 mM ammonium acetate in a 1:1 acetonitrile/methanol mixture) at a flow rate of 1 mL/min in 12 min. Under

this gradient $TpTSO_2^-$ elutes at 4.8 min, TpTOH at 7.6 min and TpT at 8.2 min. The mass signals were monitored under positive and negative ion mode respectively (41).

2.2.6 Alkylation of Cysteine 141 and Analysis

Cysteine alkylation of WT SPL or C141A mutant was carried out in 200 µL sodium phosphate buffer at pH 7.0 containing 250 mM NaCl and 10% glycerol. The protein (5 µM) was treated with 0.5 mM iodoacetamide in the dark for 1 hour. The reaction was conducted in anaerobic chamber, and the protein kept on ice through the treatment to minimize protein denaturation. The solution was then diluted by 2-fold using *dd* water, and 0.1 µL of the resulting solution injected into the Agilent 6520 Accurate-Mass Q-TOF LC/MS spectrometer. The data was acquired via Agilent MassHunter Workstation Data Acquisition (B.03.00) and analyzed via Qualitative Analysis of MassHunter Acquisition Data (B.03.00) software. The remaining protein was digested by α-chymotrypsin and trypsin overnight in 37 ˚C incubator. The resulting peptide fragments were injected into Agilent 6520 Accurate-Mass Q-TOF LC/MS and analyzed as described above. The activity of the alkylated protein was also studied under the standard procedure and analyzed by HPLC (41).

2.3 Results

Research suggests that cysteine 141 of *B. Subtilis* SPL plays a critical role in enzyme catalysis by acting as the intrinsic H atom donor to the thymine allylic radical. The following assays provide characterization of the C141A mutant, including activity

and kinetics data. All together this data confirms the importance of the C141 residue as the H atom donor in the repair process of SP by SPL.

2.3.1 C141A Expression and Purification

Containing a His_6-tag, the C141A SPL was able to be purified via Ni-NTA chromatography. SDS-PAGE shows ~90% protein purity after elution from the nickel beads. At pH 7 (pI = 8.5), and in the presence of 150 mM NaCl, the SPL protein binds tightly to SP sepharose ion exchange resin which is absolutely necessary in the purification of SPL C141A. Studies performed by Linlin Yang (Dr. Li research group) showed that when SPL was only purified by Ni-NTA chromatography, an unknown enzyme contaminates SPL protein and consumes the 5'-dA generated in the SP repair process. Thorough washing on the ion-exchange column removes this contaminating enzyme allowing for SPL C141A to be obtained at >99% purity.

2.3.2 C141A Fe-S Content Assays

The presence of the [4Fe-4S] cluster is suggested by the dark-brown coloration of the purified protein. Confirmation of the cluster is supported by the characteristic UV absorption band observed at 420 nm (Figure 2.3).

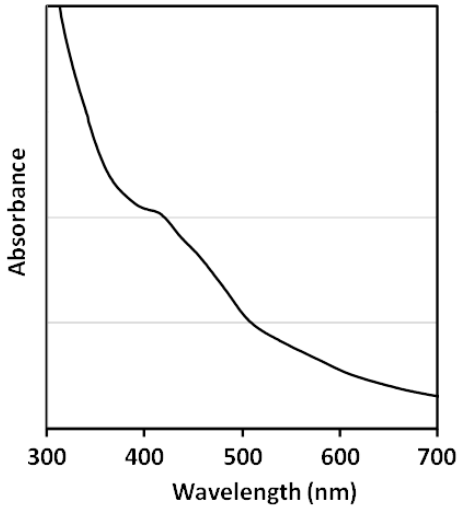

Figure 2.3: UV-Visible Spectrum of [4Fe-4S] Cluster in SPL C141A Mutant (41). 50 uM protein was utilized in a 25 mM Tris buffer containing 250 mM NaCl, 10% glycerol, at pH 7.0. The spectra were recorded in a UV cuvette with a 1 cm path length under anaerobic conditions at room temperature

Data obtained from Joshua Telser (Roosevelt University, Chicago) show that the Fe-S cluster exhibits an S = ½ signal upon dithionite reduction that is indistinguishable from the EPR signal of the WT SPL cluster. Observation of an intact Fe-S cluster confirm that the C141 residue is not involved in coordinating with the radical SAM FE-S cluster, which is in agreement with previous studies of this mutant enzyme. (40) Fe and S content analysis of the as-isolated protein indicated that each protein molecule contains 3.2 Fe and 3.0 S.

2.3.3 C141A Iodoacetamide Treatment

Understanding that the TpT radical takes an H atom from a residue able to exchange protons with the buffer, C141 in *B. subtilis* SPL is the most likely H donor.

A labeling study with iodoacetamide treatment was utilized to prove the accessibility of C141 to the solvent and thus available to act as the H atom donor to TpT.

Treatment of either native or denatured protein with iodoacetamide is commonly used to label cysteine residues in proteins (49, 50). It has previously been used to alkylate the free cysteine residues in iron-sulfur proteins APS reductase (51) and aconitase (52). If the cysteine 141 in *B. subtilis* SPL is the direct H atom donor to the thymine allylic radical (21), it must be accessible from the aqueous solution and should be readily alkylated by the iodoacetamide treatment (Figure 2.4).

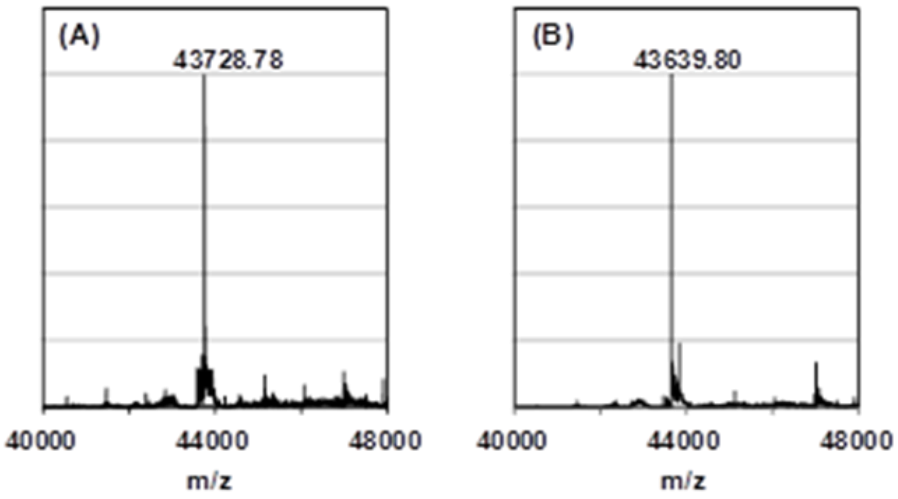

Figure 2.4: Deconvolution ESI-MS Spectrum (41) 1
Deconvolution ESI-MS spectrum of the WT SPL (A) and C141A SPL (B) enzyme treated by excess iodoacetamide under native conditions.

Deconvolution ESI-MS spectrum of the WT SPL (A) treated by excess iodoacetamide under native condition shows that when compared with the untreated WT SPL which possesses a MS of 43499.16, the treated WT SPL exhibited a mass gain of 229.62, suggesting that all four cysteine residues are alkylated. Under

the same conditions, C141A SPL(B) exhibited a mass gain of 171.31 (compared with the untreated protein, which possesses a MS of 43468.49) suggesting that all three cysteine residues in the radical SAM motif are alkylated.

To further identify that C141 is the most readily alkylated of the four cysteine residues in SPL, a time-course assay was performed to analyze the labeled species of SPL.

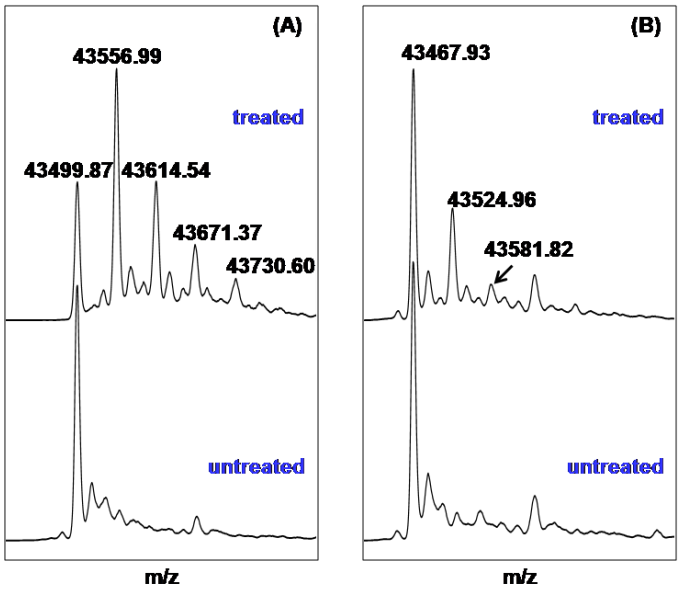

Figure 2.5: Additional Deconvolution Spectrum (41).
Deconvolution ESI-MS spectrum. (A) WT SPL treated by excess iodoacetamide under native conditions. Compared with the untreated protein, the major species of treated enzyme shows a mass gain of 57.13. The intensity of this peak is much stronger than those corresponding to proteins which carry 2, 3, or 4 labels. This observation suggests that one of the four cysteines in WT SPL is prone to alkylation. (B) SPL C141A mutant treated by excess iodoacetamide under identical conditions as WT SPL. The mono-labeled species in the treated C141A mutant exhibited a peak whose intensity is comparable with that of the treated WT enzyme carrying two alkyl labels, but much weaker than that corresponding to the mono-alkylated WT enzyme, suggesting that the alkylation site is at one of the three cluster cysteines. The different behavior toward the iodoacetamide treatment between these two proteins suggests that C141 residue in the WT SPL is accessible to the aqueous solution.

Figure 2.5 identifies the deconvolution spectra of both WT SPL and C141A SPL. After treatment with 100-fold iodoacetamide under native conditions, the WT SPL results in ~ 50% of the enzyme carrying one alkyl label, while the remaining enzyme holds 0,2,3,or 4 labels. Contrastingly, the C141A enzyme shows ~80% of the enzyme remaining unlabeled post treatment. Of the labeled C141A species, the degree of mono-alkylated protein is comparable to the di-alkylated protein in the WT enzyme, suggesting that the alkylation site is indeed at one of the three cysteines in the cluster. Trypsin digestion was used to further prove that the WT SPL contained an acetamide label at the C141 residue. This labeled fragment was absent in the SPL C141A mutant, suggesting that the C141 in WT SPL is accessible and likely to be alkylated by iodoacetamide treatment.

Cravatt *et.al*. (50) demonstrated that a fully exposed cysteine in a native protein is readily labeled by stoichiometric amounts of iodoacetamide. Our results indicate that although C141 is accessible and able to be alkylated, it must be well protected in the enzyme binding site, as treatment with 100-fold iodoacetamide only alkylated 50% of the WT enzyme. Prolonged exposure to iodoacetamide resulted in all of the cysteine residues in the WT SPL and C141A mutant being alkylated. It is unusual that the three cysteines in the radical SAM motif were alkylated, as chelation by the iron-sulfur cluster typically protects these cysteines. However, the radical SAM motif is most often located on a flexible loop at the protein surface which makes effective protection of the three cysteines less likely.

Our observations indicate that this secondary structure makes the cysteines more prone to attack by the labeling reagent.

To confirm that the alkylation of the four cysteines was not due to the denaturation of SPL during iodoacetamide treatment, the activity of the alkylated WT enzyme was tested. Although WT enzyme results in dinucleotide TpT as the SP repair product, the alkylated SPL is expected to behave similarly to the C141A mutant, which produces $TpTSO_2^-$ as the major repair product (40). Under the hypothesis that the mono-alkylated species shown in Figure 2.5 only had the C141 residue modified, the alkylated protein and unmodified WT SPL were present in a ~5:3 ratio. Activity assays demonstrate that the WT SPL repairs SP ~ 3-fold faster than the C141A mutant, therefore TpT/$TpTSO_2^-$ should be produced under a ~2:1 ratio. It was observed that the isolated TpT/$TpTSO_2^-$ was present in a mole ratio of 2.5:1 (48), suggesting that the SPL displaying an alkylated cysteine 141 remains in its native state, and that the C141 in WT SPL is accessible to the aqueous buffer.

2.3.4 C141A Activity Assays

SPL C141A Reaction with Regular SP TpT

Iodoacetamide treatment proves that C141 is accessible to the TpT radical, making it the likely H atom donor. However, what other protein residues may be involved in the H atom transfer process. Structural data (Figure 3.1) shows that a conserved tyrosine (Y99 in *B. subtilis* SPL) is only 4.3 Å from the SP methylene carbon,

making it another candidate for H atom donation. If this tyrosine is involved in the H atom transfer process, this residue would still be present in the C141A mutant. As C141A is expected to produce TpT as the repair product for at least the first enzyme turnover, a lag phase in the formation of $TpTSO_2^-$ would be expected.

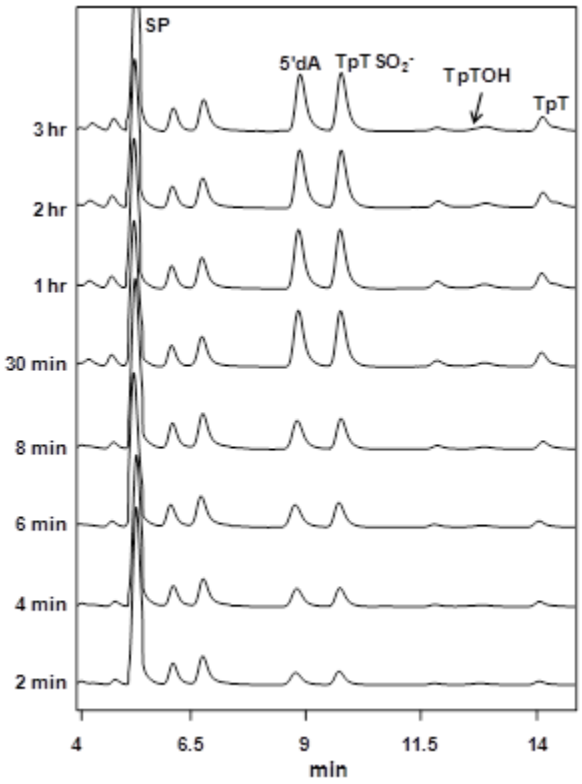

Figure 2.6: HPLC Chromatograph of SP TpT Repair Process (41).
HPLC chromatograph of the SP TpT repair process mediated by the *B. subtilis* SPL C141A mutant with 30 µM enzyme, 150 µM SAM and 1 mM dithionite. Under the HPLC program, the SP TpT was eluted at 5.4 min, 5'-dA at 8.9 min, $TpTSO_2^-$ at 9.8 min, TpTOH at 12.9 min and TpT at 14.1 min. Linear formations of $TpTSO_2^-$ and TpT were observed in the first 30 minutes of the reaction. The TpTOH peak overlapped with an uncharacterized compound in our HPLC chromatograph. The yield of TpTOH was too low to be determined.

Kinetic studies of the SPL C141A found that in the absence of DTT and the presence of 1 mM sodium dithionite, $TpTSO_2^-$ was isolated as the major product, and

TpT a minor product. TpTOH was also detected in extremely low amounts (<0.1%) (Figure 2.6). The formation rates of each product were calculated based on calibration curves constructed with authentic TpT and $TpTSO_2^-$, and are shown in Table 1.

Table 1: Formation Rates (min^{-1}) of TpT $TpTSO_2^-$ and TpT in C141A mutant reaction (1 mM sodium dithionite, 0.1 mM SAM and varying concentrations of DTT as the H atom donor) (41).

	No DTT	1 mM DTT	10 mM DTT
$TpTSO_2^-$	0.11 ± 0.01	0.11± 0.01	0.05 ± 0.005
TpT	0.014 ± 0.002	0.019 ± 0.002	0.041 ± 0.005
$TpTSO_2^-$ + TpT	0.12 ± 0.01	0.13 ± 0.01	0.09 ± 0.01

These studies performed by Linlin Yang, revealed that $TpTSO_2^-$ and TpT formed under constant reaction rates from the initiation of the reaction with no observable lag phase in the formation of $TpTSO_2^-$ (Figure 2.6). This evidence implies that no other protein residue is located between the TpT radical and the C141 in the WT SPL reaction pathway. The activity of C141A mutant on the dinucleotide SP yielded multiple turnovers and showed that > 70% of the repaired SPs rendered the $TpTSO_2^-$ adduct, with TpT as a minor species in the repair activity observed.

The following studies of TpT formation in the C141A SPL reaction were performed by Linlin Yang of Dr. Li's research group, and are included here as they provide context to the discussion following in this chapter.

TpT Formation in SPL C141A Reactions

The production of TpT in the absence of what we believe to be the intrinsic H atom donor is interesting. One possibility is that the H atom is supplied to the TpT radical from a small molecule in the reaction buffer. Tris was excluded as the possible H atom donor, as the same reaction pattern was observed when phosphate buffer was used in the C141A reaction. Due to the supplementation of thiol compounds in radical SAM reactions, the C141A SPL reaction was performed in varying concentrations of DTT. As seen in Table 1, with equal amounts of dithionite and DTT (1 mM), there was little noticeable difference in both TpT and $TpTSO_2^-$ formation. However, in the presence of 10 mM DTT, the TpT formation rate increased 3-fold, but the formation of $TpTSO_2^-$ and the overall SP repair rate were slower.

Dithionite reduces the $[4Fe\text{-}4S]^{2+}$ cluster through an outer-sphere electron transfer process; the partial inhibition of the SP repair reaction may be due to the excess DTT blocking the enzyme binding pocket, which prevents the dithionite access to the cluster. Although the overall reaction rate is slowed by concentrated DTT, the increased yield of TpT suggests that the presence of an H atom donor could facilitate the formation of TpT. However, this TpT enhancement requires a large amount of DTT. In our enzyme reaction, no small molecule is present in a 10 mM concentration, therefore donation of H atom from a small molecule can be ruled out.

SPL C141A Reaction with Varying Amount of Dithionite

A second possibility for the formation of TpT in the C141A mutant is that another protein residue, such as tyrosine Y99, may donate an H atom to the TpT radical. To test this theory, enzyme reactions were carried out with varying concentrations of dithionite. Dithionite plays dual roles in the SPL C141A reaction: 1) reducing the $[4Fe\text{-}4S]^{2+}$ cluster to initiate the SAM cleavage reaction, and 2) quenching the thymine radical to yield $TpTSO_2^-$. If the needed H atom is supplied by the protein, the availability of the H atom would be unchanged. Under low dithionite concentrations, the formation of $TpTSO_2^-$ would be unfavorable due to the lack of reactant, and an increase in the production of TpT should be observed.

To investigate the quenching effect of dithionite on the SP repair reaction, varying amounts of dithionite or 10 mM DTT (as the radical quenching reagent) along with SP and SAM were incubated with C141A that had been pre-reduced (large excess of dithionite subsequently removed by desalting columns prior to reaction). Table 2 shows that under low dithionite concentration, $TpTSO_2^-$ becomes an even more dominating repair product. The observed trend, as shown by the $TpTSO_2^-$/TpT ratio, was that formation of TpT became more favorable as dithionite concentration increased, until comparable amounts of $TpTSO_2^-$ and TpT were observed at 10 mM dithionite concentration. If another protein residue were the H atom donor, we would expect an opposite trend for the $TpTSO_2^-$/TpT vs. dithionite concentration. As such, we conclude that TpT formation is directed by dithionite,

and therefore the TpT found in the C141A mutant reaction is not generated through direct H atom transfer as is seen in WT SPL reaction (21).

Table 2: $TpTSO_2^-$/TpT Ratio Found in (A) the SP Repair Reaction.
Facilitated by pre-reduced C141A mutant (10 μM) supplemented by varying amount of dithionite or DTT, and (B) photoreaction of TpTSPh (1 mM) supplemented by varying amount of dithionite (41).

Dithionite (mM)	0.02	0.05	0.2	1	10	10 mM DTT
$TpTSO_2^-/TpT^A$	7.1 ± 1	5.8 ± 0.6	3.2 ± 0.3	2.8 ± 0.3	1.8 ± 0.3	<0.1
$TpTSO_2^-/TpT^B$	0.08 ± 0.01	0.14 ± 0.01	0.18 ± 0.02	0.21 ± 0.02	0.44 ± 0.03	0.22 ± 0.02^C

TpT is not Produced via $TpTSO_2^-$ Decomposition

A third scenario for formation of TpT in C141A mutant reactions is via $TpTSO_2^-$ degradation (Figure 2.7). To explore this possibility $TpTSO_2^-$ was incubated with enzyme in pH 7.0 buffer for 1 hour. HPLC analysis revealed that no TpT resulted. Nor was any TpT present after additional experiments in pH 7.0 and 9.0 Tris buffer in the presence or absence of UV light respectively, as the neutral or mildly basic condition is supposed to favor the SO_2 elimination (53-55). These results suggest that $TpTSO_2^-$ degradation is not the cause of TpT found in the C141A reaction, and that the TpT must originate directly from the TpT radical.

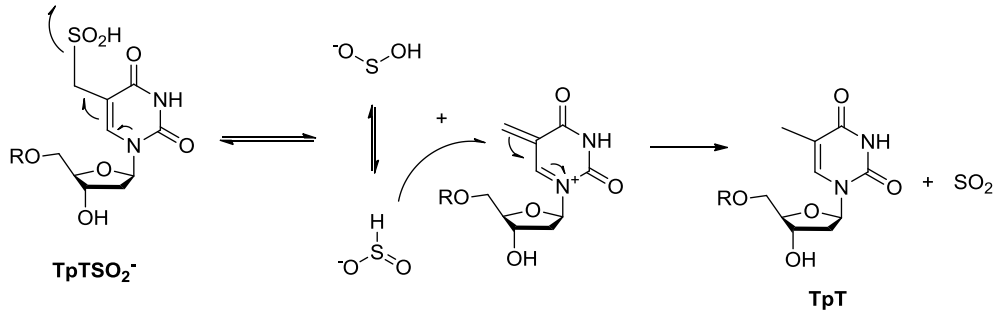

Figure 2.7: Mechanism for $TpTSO_2^-$ Degradation (41).

Consumption of SAM and Formation of 5'-dA

The ratio of *5'*-dA and product is of great significance in radical SAM enzyme reactions. A ratio of 1:1 indicates that SAM is a co-substrate and is consumed after each catalytic turnover, while a 1:X (X>1) suggests that SAM is regenerated after each catalytic cycle and therefore acts as a cofactor.

Figure 2.8 (B) tracks the consumption of SAM and subsequent formation of *5'*-dA, as well as the appearance of the repaired products. The ratio between consumed SAM (formed *5'*-dA) and reacted SP was 1.08 ± 0.1, indicating that SAM acts as a co-substrate in the SPL C141A reactions. As a comparison, the ratio of *5'*-dA to TpT was monitored in SPL WT reaction and resulted in 1.5 ± 0.2. Side by side, the differences between the WT SPL and C141A reactions are apparent. These results suggest that SAM plays a partially catalytic role (as a cofactor) in the WT SPL reaction but has a noncatalytic role (co-substrate) in the C141A mutant.

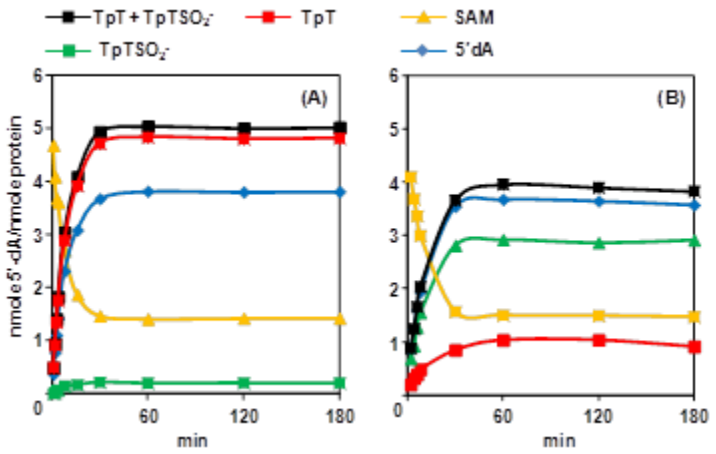

Figure 2.8: Formation of TpT, $TpTSO_2^-$, *5'*-dA (41).
(A) The formation of TpT, $TpTSO_2^-$, *5'*-dA as well as the consumption of SAM in the WT SPL reaction. 5 equivalents of SAM were added to initiate the reaction. A background level of $TpTSO_2^-$ was observed along with the formation of TpT. The ratio between the SP repair products (TpT +$TpTSO_2^-$) and *5'*-dA is found to be 1.5 : 1 for the WT SPL reaction, suggesting that SAM is partially catalytic here. (B) The formation of TpT, $TpTSO_2^-$, *5'*-dA as well as the consumption of SAM in the SPL C141A reaction with 5 equivalents of SAM supplemented. The ratio between the SP repair products (TpT +$TpTSO_2^-$) and *5'*-dA was found to be 1.08 : 1 for the SPL C141A reaction, suggesting that SAM plays a non-catalytic role in the C141A reaction and is a co-substrate. Under the 5 equivalents of SAM, the SP TpT repair rate by WT SPL was determined to be 0.41 ± 0.03 min^{-1}, and by SPL C141A mutant was determined to be 0.14 ± 0.02 min^{-1}.

SPL C141A Reaction in the Absence of Excess Reductant

Being able to reliably measure the amount of yielded *5'*-dA provides us a marker to accurately determine the reaction turnover numbers. In our previous report, after using desalting column to remove the excess dithionite, the pre-reduced cluster of WT SPL was found to support 12 turnovers under ~3 equivalents of SAM (55). *Using our latest calibration curve, the number is now determined to be 5.4*. This number still suggests that the WT SPL reaction has a closed catalytic cycle and is consistent with our latest results here.

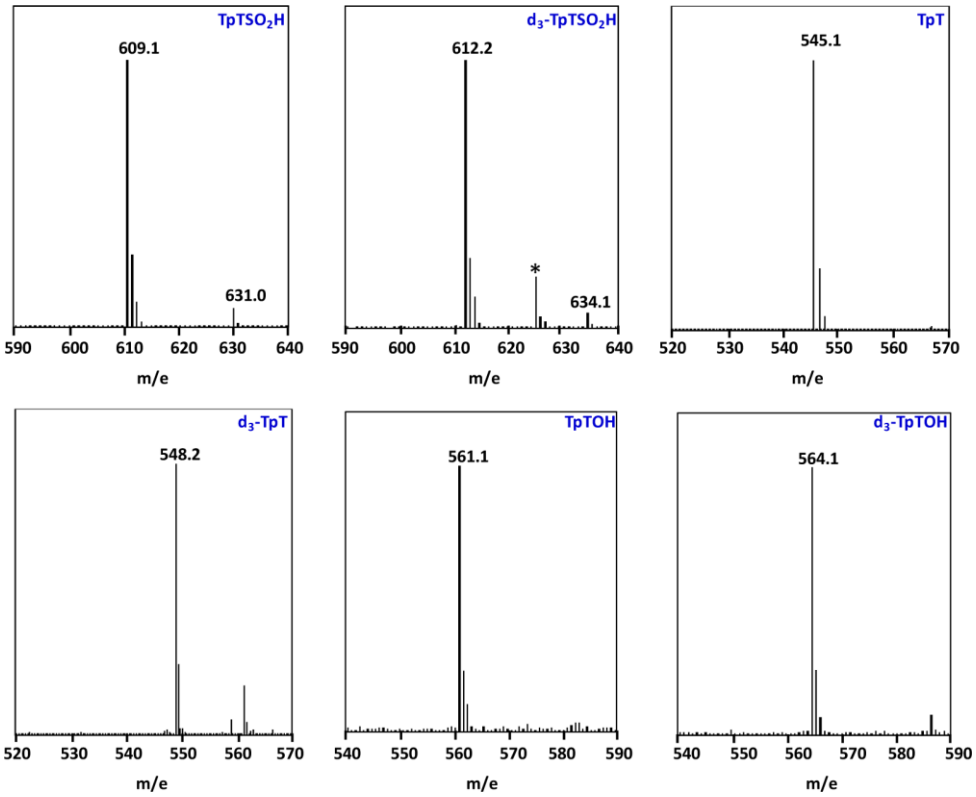

Figure 2.9: $[M-H]^-$ Signals of Repair Products (41).
$[M - H]-$ signals of TpT, $TpTSO_2^-$, and TpTOH isolated from the SP TpT and d_4-SP TpT repair reactions mediated by the SPL C141A mutant. The deuterium abstracted from the d_4-SP TpT during the repair process is not returned to the products, and the corresponding d_3 species were isolated for all three products. The asterisk denotes an impurity in the ESI-MS spectrum of d_3-$TpTSO_2^-$.

Linlin Yang performed similar experiments with the C141A mutant to test if the C→A mutation disrupts such a cycle. After pre-reduction with dithionite for 30 min, the resulting $[4Fe\text{-}4S]^+$ cluster in SPL C141A mutant supported only ~0.4 turnover, with TpT the dominant product when 10 mM of DTT was supplemented. No turnover was observed in the absence of DTT, suggesting that being able to quench the TpT radical is the pre-requisite for the occurrence of the SP repair reaction. Other thiol compounds can also rescue the SPL C141A reaction, but the

yield of TpT would be even lower. The low concentration of DTT (< 1 mM) has little effect to stimulate the reaction, suggesting that the thymine radical is well protected by the enzyme against external H donors. This finding is consistent with the result obtained in the C141 labeling studies described above that C141 appears to be protected in the enzyme binding pocket. As participants for the key H atom transfer process during the SP repair process, both the TpT radical and the C141 are protected by the SPL enzyme.

The 0.4 turnover could be due to the incomplete reduction of the radical SAM cluster upon the 30-minute dithionite treatment. As shown by our previous EPR experiment, a 30-minute reduction led to only ~ 40% of SPL cluster reduction; 1 hr. reduction resulted in ~ 70% of the cluster being converted to the +1 oxidation state (21). The observation is in line with the 20% $[4Fe\text{-}4S]^{+}$ cluster reduction observed by Broderick (57) and the 40% cluster reduction by Knappe (58) in PFL-AE studies upon prolonged reduction. More importantly, the difficulty for the externally added thiol to be correctly positioned to quench the TpT radical may play a major role for the low yield of TpT as under an identical condition, > 5 turnovers were observed for the WT SPL reaction (21). Nevertheless, the < 1 turnover in the C141A mutant suggests that the C141A mutant no longer possesses a closed catalytic cycle.

SPL C141A Reaction with d_4-SP TpT as the Substrate

The WT SPL enzyme takes the H_{6proR} atom to initiate the SP repair reaction, the abstracted H atom however is not returned to the TpT product. In the aqueous

buffer, the repair of d_4-SP TpT by WT SPL leads to the formation of d_3-TpT. As shown in Figure 2.9, all three products, $TpTSO_2^-$, TpT, and TpTOH, from the d_4-SP TpT repair reaction mediated by the C141A mutant contain only three deuteriums, suggesting that the abstracted deuterium by the 5'-dA• was not returned as expected. The C→A mutation disturbs the H-atom back-donation step and the steps after, but likely leaves the previous steps intact.

Linear formation against reaction time can be obtained for $TpTSO_2^-$ and TpT species under a saturated substrate concentration; comparing the correspondent rates using d_0- and d_4-SP TpT as substrates reveals the $^DV_{max}$ KIE to be 1.7 ± 0.2 for $TpTSO_2^-$ and TpT respectively (Table 3). The identical KIEs for TpT and $TpTSO_2^-$ suggest that these species share the same rate determining step. Thus the $^DV_{max}$ KIE for the C141A mutant reaction can be reported as 1.7 ± 0.2, which is smaller than the KIE of 2.8 ± 0.3 exhibited by the WT enzyme (21).

Table 3: Rates of Formation (min^{-1}) of $TpTSO_2^-$ and TpT and V_{max} KIEs in SPL C141A (41)

		Without DTT			With 1 mM DTT	
Substrate	SP TpT	d_4 SP TpT	V_{max} KIE	SP TpT	d_4 SP TpT	V_{max} KIE
$TpTSO_2^-$	0.1 ± 0.01	0.055 ± 0.005	1.78	0.1 ± 0.01	0.055 ± 0.005	1.70
TpT	0.02 ± 0.002	0.012 ± 0.001	1.67	0.026 ± 0.003	0.015 ± 0.002	1.73
$TpTSO_2^-$ and TpT	0.12 ± 0.01	0.067 ± 0.006	1.76	0.126 ± 0.013	0.07 ± 0.007	1.71

2.4 Discussion

2.4.1 C141A is Likely the H Atom Donor

To donate the H atom directly to the thymine allylic radical, the C141 –SH moiety must be accessible to the substrate. Our observation that the C141 residue can be alkylated by iodoacetamide under the native condition suggests that this cysteine is solvent accessible and should be readily available to the thymine radical. The similar behaviors of WT SPL and SPL C141A mutant under the iodoacetamide treatment suggest that the C→A mutation is unlikely to change the protein structure.

Should the C141 not be the direct H atom donor, but pass the H atom to another protein residue (Y99, for instance) during the course of the catalysis, the residue would also possess a weak X-H bond, which is perfectly positioned for the H atom transfer to the TpT radical.

Different from the class I ribonucleotide reductase, where the radical species has to be passed to the substrate binding pocket before the ribonucleotide modification reaction is initiated (59, 60), the radical chain in the SPL reaction is initiated from the substrate. Given the weak bond dissociation energy (BDE) for the protein residues which are known to be involved in the radical relay process, should a protein residue other than C141 (for instance, the Y99) serve as the direct H atom donor, an H atom would be readily available to the TpT radical, producing TpT during the first turnover. Such a hypothesis is against our observations here as the

formations of TpT and $TpTSO_2^-$ are linear from the very beginning of the SP repair reaction, suggesting that both species form at the same time.

Furthermore, should the putative residue be responsible for H atom donation, an X• radical will be left behind on this residue. Consequently, the enzyme is likely to be modified (formation of a SO_2^- adduct, for instance) in order to quench this X• as the electron transfer chain is broken after the C→A mutation. However, the C141A protein is not modified after the reaction, as proved by the ESI-MS analysis. Thus, even though our data tell us nothing about the proximity between the C141 and the TpT radical, it is extremely unlikely for a residue other than the C141 to directly donate an H atom to the TpT radical.

2.4.2 Formation of Three SP Repair Products

Among the three products $TpTSO_2^-$, TpT, and TpTOH formed in the SPL C141A reaction, the $TpTSO_2^-$ likely forms via a radical recombination reaction as discussed above. The radical replacement mechanism may also play a very minor role in its formation.

The formation of TpT is more interesting. Although TpT is produced in both SPL WT and C141A mutant reactions, it likely forms via different mechanisms. In WT SPL reaction, the –SH moiety on C141 likely donates an H atom to the thymine radical to form TpT. Such a low energy H donor is no longer present in the C141A mutant unless the reaction solution is supplemented by a large amount of thiols. As revealed by our thymine allylic radical activity studies, such a radical readily

undergoes disproportionation and reduction reactions, with reaction rates likely comparable to the radical recombination reaction (61). Actually, the fact that the presence of large excess of thiol compounds has little impact to the TpT formation further suggests that the H atom abstraction is an unfavorable reaction due to the relatively slow reaction rate (61). A reduction of thymine radical is the most likely thymine formation mechanism here, which is likely involved in the TpT formation in C141A reaction as well.

However, a direct reduction of the thymine allylic radical is unfavored as the resulting thymine methyl anion is extremely unstable, which makes the thymine radical cation reduction the most favorable mechanism (61). Since the reaction is conducted in water, the thymine C4=O bond must readily associate with a proton through the hydrogen bonding interaction with the aqueous solvent. Reducing the resulting TpT radical cation would generate TpT (Figure 2.10). Such a radical cation reduction mechanism (proton coupled electron transfer) has not received much attention before in the DNA biochemical studies (63-65). The data here argue that the thymine cation radical reduction pathway may play an important role in the thymine damage repair, which has been largely overlooked in the past.

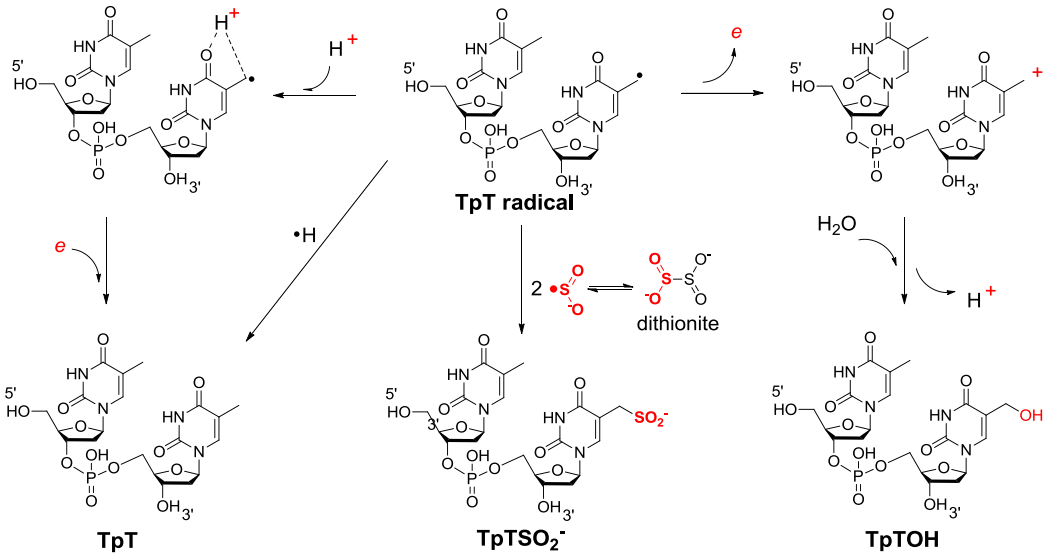

Figure 2.10: TpT Repair Pathways (41).

As shown in Table 2, in the SPL C141A mutant reaction, the $TpTSO_2^-$ is the dominating product. The cation radical reduction to produce TpT is relatively unaffected when the dithionite concentration increases while the formation of $TpTSO_2^-$ becomes more competitive due to the availability of more reactants. In contrast, the TpT radical is well protected in the C141A binding pocket, as suggested by the observation that a large amount of externally added DTT (10 mM) is needed in order to quench the TpT radical. As shown by the CPD photolyase structure, the thymine C4=O bond is recognized by a protein residue via the hydrogen bonding interaction (66). A similar recognition pattern is expected here. The pre-organized enzyme–substrate complex likely hinders a proton from the solvent to adopt the right position to associate with the allylic radical as shown in Figure 2.10, thus slowing down the TpT formation and making the $TpTSO_2^-$ formation the favorable reaction.

Dithionite is likely to serve as the electron donor in SPL C141A mutant reaction to facilitate the formation of TpT. However, we cannot exclude the possibility that the protein harbored $[4Fe\text{-}4S]^{+}$ cluster donates the needed electron. Nevertheless, the *TpT likely forms via a proton coupled electron transfer process in the SPL C141A mutant, which is different from the H atom transfer mechanism in the WT SPL reaction*.

TpTOH was isolated in previous thymine oxidation studies, its formation is typically induced by the oxidation of TpT allylic radical by either addition of O_2 (67) or radical recombination with a •OH radical (68). Our latest data suggests that it can also be produced via a thymine radical disproportionation reaction (61). As the enzyme reaction was conducted anaerobically, O_2 can be ruled out, making the radical disproportionation the most likely mechanism. The thymine cation then reacts with water to produce TpTOH (Figure 2.10). Under the reducing conditions adopted in the enzyme reaction, the thymine cation must be reductively quenched. Consequently, only a small amount of TpTOH was produced.

2.4.3 Enzyme Activity and Kinetic Isotope Effect

The bond dissociation energy (BDE) of the cysteine S-H bond is suggested to be ~3-4 kcal/mol lower than the allylic C-H bond (37,38,69,70). Assuming that the SPL configuration is such that the C141 is at the vicinity of the thymine allylic radical, the H atom back transfer step must be heavily favored and should not affect the overall SP repair rate. In contrast, the C→A mutation removes this natural H atom

transfer process; the TpT allylic radical has to either be released before it is quenched or wait until a quenching reagent diffuses into the enzyme binding pocket to react with the radical and generate a stable product. Such a quenching step must be slow, resulting in the ~ 3-fold rate reduction exhibited by the C141A mutant relative to that of the WT enzyme (Figure 2.8).

Theoretical calculations suggest that the two steps involved in the H-atom exchange with 5′-dA possess the highest energy barriers (37,38,71,72). Of these two steps, the H-atom back-donation step has the higher barrier due to the energy difference between the allylic radical and the C-H bond associated with the methyl moiety of 5′-dA. Although our data suggests that it is the –SH moiety of C141, not the –CH3 of 5′-dA, that serves as the H atom donor for the thymine allylic radical, the resulting protein radical(s) are likely to be stable as well. The regeneration of the 5′-dA• is expected to be slow (33,74). Thus, it is reasonable to hypothesize that the rate-determining step in SPL reaction is the regeneration of 5′-dA•; all steps before, including the H atom abstraction by the 5′-dA• from the C6 carbon of SP to obtain the SP radical, belong to the ″rate-determining zone″ (75). The rate constants from all steps in this zone will contribute to the V_{max} KIE (75-77).

The intrinsic isotope effect caused by the reaction between the 5′-dA• and the deuterated SP substrate is likely to be "diluted" by other steps in this zone, resulting in a moderate V_{max} KIE of 2.8 for the WT SPL reaction (21).

The rationale above assumes that SAM is regenerated after every catalytic cycle. However, the observed TpT/5′-dA ratio of 1.5 suggests that the roughly two thirds of the formed 5′-dA and methionine molecules exchange with SAM from the environment during the SPL catalysis. Currently, no data is available to help us determine how fast this exchange step is. However, it is clear that the reaction rates we observed here seem to be the average of two reactions: one results in the SAM regeneration, the other results in the exchange of 5′-dA and methionine with SAM. Therefore, the V_{max} KIE here is unlikely to represent the true V_{max} KIE occurring in vivo. To determine the V_{max} KIE for the *in vivo* reaction, a method has to be found to prevent the SAM/*5′*-dA-methionine exchange from occurring.

Such a moderate V_{max} KIE is further reduced in the C141A mutant reaction due to the slower thymine radical quenching process. Although changing the SP TpT to deuterated d_4-SP TpT slows down the SP repair reaction, the repair rate was reduced to a less extent, resulting in a V_{max} KIE of 1.7 ± 0.2 for both $TpTSO_2^-$ and TpT formations. The almost identical KIE exhibited by these two products indicates that despite the different quenching mechanism, the reaction rates for this step must be similar. Comparing with the WT SPL,(21) the reduced V_{max} KIE in the mutant reaction

suggests that the H abstraction step by *5′*-dA• becomes even less rate-determining (78). The radical quenching step likely becomes the new rate-limiting step, as the SAM regeneration process is no longer possible. However, in C141A reaction, SAM exchanges with the formed 5′-dA and methionine at the end of each catalytic cycle. Should this step be rate-determining, a slower TpT radical quenching step can still lead to the reduced V_{max} KIE as observed here.

2.4.4 SAM Regeneration

To recycle SAM after each turnover is probably the most efficient choice for the germinated spores. UV irradiation can convert as much as 8% of the total thymine in bacterial genomic DNA to SP;(15,16) these SPs must be repaired by SPL for the bacteria to survive (18,17,79). Germinated spores have many urgent needs in resuming their normal life cycle with limited resources, to make good use of every SAM molecule must be important. The *in vitro* reactions under a large excess of SAM reported here are unlikely to happen *in vivo*.

Despite the potential importance of SAM regeneration for *in vivo* reaction, such a process is not fully established by *in vitro* experiments. Previous efforts to establish the SAM regeneration were conducted via a tritium labeling experiment in SPL and lysine-2,3-aminomutase (LAM) (32,33, 80). In both cases, the percentage of label transfer from the substrate into SAM was suggested to be very low (21,81,82). Recent proposals by Eguchi in the studies of BtrN (83) and by Liu in the studies of DesII,(84) both of which are radical SAM enzymes, suggested that SAM cleavage, as

well as the subsequent H atom abstraction by the *5*′-dA• from enzyme substrates, may be reversible. Such reversible processes could explain the tritium incorporation into SAM as previously observed in SPL reaction (66).

SAM becomes a co-substrate in the C141A reaction. This is reasonable considering that C141 is a part of the catalytic pathway; disrupting this pathway makes the closed catalytic cycle open. In WT SPL reaction, the TpT/5′-dA ratio of 1.5 ± 0.1 suggests that only one third of SAM behaves like a co-factor. We'd like to observe the SAM regeneration in a more significant scale; however, this seems unlikely using the dinucleotide SP TpT as the enzyme substrate.

The small regeneration scale predicted here highlights the difficulty to directly detect the SAM regeneration process. In B-12 enzymes, where no excess B-12 cofactor is needed, the 5′-dA recycling process can be readily observed. In contrast, the binding of SAM to radical SAM enzyme is weak; to achieve enough enzyme activity, 2-3 equivalents of SAM is needed (21,32). This then determines that there are always excess SAM molecules available in the reaction buffer, which can readily exchange with the yielded *5*′-dA and methionine, making the SAM recyclization unnecessary. To study the SAM regeneration process, a limited SAM supply is required. In addition, the enzyme has to bind SAM (*5*′-dA and methionine) tightly. Such a condition may be achievable by using a tightly bound SP substrate. As shown in Broderick's experiments, using a SP containing plasmid DNA, one equivalent SAM can support > 500 turnovers (32). How a tighter substrate binding enhances the SAM recyclization is currently unclear.

How is SAM regenerated in the WT enzyme? Cysteine based thiyl radical is known to abstract an H atom from 5′-dA in class II ribonucleotide reductase (RNR) to produce the 5′-dA• before it recombines with cobalamin to regenerate the adenosylcobalamin at the end of each catalytic cycle (85). However, in class II RNR, the 5′-dA• interacts only with the active-site cysteine and does not associate with the substrate at any point of the catalytic cycle. In contrast, in SPL, the 5′-dA• abstracts the H_{6proR} atom of the *5*′-T of SP to initiate the repair reaction;(20) while the C141 likely provides the needed H atom to the methyl radical at the *3*′-T to generate the repaired TpT. Should the thiyl radical on C141 be directly responsible for H atom abstraction from *5*′-dA to regenerate SAM, the TpT would be released first, followed by a major protein conformational change before the thiyl radical can interact with the 5′-dA. On the other hand, it is reasonable for the thiyl radical to oxidize a neighboring protein residue before the reaction with *5*′-dA occurs. In that case, SPL must harbor an electron transfer pathway with the C141 a key element.

2.4.5 Alternative Route for SAM Regeneration

Although the SAM regeneration is the most reasonable hypothesis, we cannot rule out other possibilities for the SPL catalyzed SP repair reaction. For instance, what if the 5′-dA generated from the SAM reductive reaction is responsible only for the first catalytic cycle and the protein radical generated takes over and catalyzes the rest of the turnovers? Under in vitro conditions, the presence of excess SAM and reductant determines that both catalytic routes may occur.

The mechanistic studies of SPL thus far suggest that the enzyme reaction can be divided into two half reactions: SP repair/TpT formation and SAM regeneration. These two half reactions are tightly coupled under a low SAM concentration in vivo; but are uncoupled under sufficient SAM supply. Progress has been made in elucidating the half reaction involved in SP repair and TpT formation; however, the other half - SAM regeneration, remains largely unclear. Chapter 3 will take a look at two conserved tyrosine residues in SPL WT (Y97, Y99) that are believed to play a role in SAM regeneration.

This research confirms initial suggestions indicating the involvement of a protein residue in the H atom back donation to the *3'*-T methyl group to complete the repair of SP TpT. C141 is this intrinsic H atom donor as proved by: iodoacetamide labeling assays showing the accessibility of C141 to solvent and thus TpT; the reduced repair rate and KIE indicating a significant interruption in the closed catalytic cycle of SP repair by this C→A mutation; and the formation of $TpTSO_2^-$ as the major product of repair when the H atom back donation is not possible due to the alanine mutation in this critical C141 residue.

2.5 Acknowledgements

The research discussed in this chapter was a collaborative effort of many individuals to whom credit must be given. Special thanks to Linlin Yang, Gengjie Lin, Yajun Jian, Joshua Telser and Lei Li for all of their hard work and dedication to this

project and the publication. “Mechanistic Studies of the Spore Photoproduct Lyase (SPL) via a Single Cysteine Mutation”. Biochemistry. 2012 Sep 11;51(36):7173-88.

CHAPTER 3. "A RADICAL TRANSFER PATHWAY IN SPORE PHOTOPRODUCT LYASE"

3.1 Introduction

As discussed in Chapter 2, evidence suggests that the C141 residue in *B. subtilis* (*Bs*) SPL (21,39,40,41) is the intrinsic H atom donor in the repair process of SP. This mechanism is supported by recently solved crystal structures of wild-type (WT) and mutant SPL from *bacterium Geobacillus thermodenitrificans* (*Gt*) which were solved by Benjdia *et.al.* (Figure 3.1) (48). The structure shows that there is 4.5 Å between the methylene bridge of the dinucleoside SP and the conserved cysteine, which is close enough for the cysteine to be the direct H atom donor. There is ~77% conserved sequence identity between $SPL_{(Gt)}$ and $SPL_{(Bs)}$, however $SPL_{(Gt)}$ exhibits a -1 sequence shift.

The *Gt* SPL structure (Figure 3.1) is changed neither by $C140A_{(Gt)}$ nor the isoteric $C140S_{(Gt)}$ mutation. Evidence that the conserved cysteine must be the intrinsic H atom donor to the substrate radical (41) is demonstrated by enzyme kinetic studies of SPL $C141A_{(Bs)}$ mutant as demonstrated in Chapter 2. In the WT SPL reaction donation of this H atom by C141 then results in a thiyl radical on the C141 residue of SPL WT. This C141-S• must be involved in the process of SAM regeneration.

Crystal structure evidence provided by Benjdia *et.al.* (Figure 3.1) also identifies two conserved tyrosines (Y97 and Y99 in *B. subtilis*) in the active site of SPL. The Y99 residue is perfectly positioned to be involved in the H atom transfer (HAT) process to the thiyl radical on this cysteine, indicating that Y99 must be a contributor to the regeneration process of SAM at the end of each catalytic cycle (21,32). This report presents experimental evidence suggesting that in addition to the cysteine, two tyrosines are also key for catalysis.

To investigate the roles of Y97, Y99 of *B. subtilis* in the catalytic cycle of SPL, I expressed and purified two SPL mutants (Y97F, Y99F). Following confirmation of the presence of the [4Fe-4S] cluster (UV 420nm, Fe-S assays), I performed activity and kinetic isotope effect assays to determine the effects of these Y→F mutants on the rate of SP repair and to identify the role of each in SP repair by SPL.

3.2 Experimental Methods

3.2.1 Expression and Purification of SPL Mutants

Both the WT enzyme and the tyrosine mutants for $SPL_{(Bs)}$ were expressed in LB (Luria Bertani) medium containing the antibiotics ampicillin (100 μg/mL) and kanamycin (25 μg/mL) as previously described (21). The proteins were purified via Ni-NTA chromatography followed by an ion exchange chromatography using the SP Sepharose fast flow ion exchange resin (GE Healthcare Life Sciences, Piscataway, NJ). The bound protein was washed using a buffer containing 25 mM Tris, 250 mM NaCl and 10%

glycerol (pH 7.0) for 10 column volumes. The protein was then eluted using the same buffer containing 500 mM NaCl instead. The resulting protein was diluted 2-fold to reduce the salt concentration to 250 mM and saved for activity studies.

The expression and purification conditions used for the SPL $Y98F_{(Gt)}$ mutant protein were similar to the WT enzyme (48). The harvested cells were re-suspended in buffer A (50 mM Tris–HCl pH 8, 500 mM NaCl, 10 mM $MgCl_2$, 10% glycerol) supplemented by 5 mM 2-mercaptoethanol, 1 tablet of protease inhibitor cocktail (Complete, EDTA-free, Roche), 4 $\mu g.mL^{-1}$ of DNase I (Roche), 4 $\mu g.mL^{-1}$ of RNase (Roche) and 0.1 $mg.mL^{-1}$ lysozyme (Sigma-Aldrich) and disrupted by sonication. After ultracentrifugation, the supernatant was loaded on a Ni-NTA (Qiagen) gel column equilibrated with buffer A containing 20 mM imidazole (Sigma-Aldrich). The mutant protein was eluted with 500 mM imidazole which was then removed by a desalting column (Sephadex G-25, GE healthcare).

The SPL $Y98F_{(Gt)}$ protein was further purified by heparin affinity column chromatography (GE Healthcare) using 50 mM Tris–HCl at pH 8, 300 mM NaCl, 1% glycerol and 3 mM dithiothreitol.

3.2.2 Protein, Iron and Sulfide Assays

Routine determinations of protein concentration were conducted by the Bradford method (44), using bovine gamma globulin as the protein standard. Protein concentrations were calibrated on the basis of the absorption of aromatic residues at 280 nm in the presence of 6 M guanidine hydrochloride using the method of Gill and

von Hippel using the value of 37460 for the molar absorptivity coefficient for SPL(45). Iron content was determined using *o*-bathophenanthroline (OBP) under reductive conditions after protein digestion in 0.8% $KMnO_4$ and 1.2 M HCl as described by Fish (46). Sulfide assays were carried out using the method described by Beinert (47).

3.2.3 Enzyme Activity Assay

Typically, a reaction mixture contained 30 μM $SPL_{(Bs)}$ enzyme (or tyrosine mutant), 1 mM SP TpT substrate, and 150 μM SAM in a final volume of 400 μL of buffer containing 25 mM Tris-HCl, 300 mM NaCl and 10% glycerol at pH 7.0. Sodium dithionite (final concentration 1 mM) was added as a reductant to initiate the enzyme reaction. The reactions were carried out under anaerobic conditions at ambient temperature for various periods of time. Under the conditions of the assay, the formation of TpT was linear with time for up to 15 min. At each time point, 90 μL of the solution was taken out to an Eppendorf tube and quenched by 10 μL of 3 M HCl (42).

After removing the protein residues via centrifugation at 15,000 rpm for 20 min, the resulting supernatant was loaded onto HPLC, separated and analyzed as described (21).

3.2.4 Deuterium Kinetic Isotope Effects (KIEs)

The V_{max} KIEs for the WT $SPL_{(Bs)}$ and $C141A_{(Bs)}$ mutant were reported in previous publications (21,41). The V_{max} KIEs for both Y/F mutants were determined in a similar manner by direct comparison of the initial rates with 1 mM of SP TpT and d_4-SP TpT

respectively. The V_{max}/K_m KIEs were measured by competition experiments in which an equimolar mixture of SP TpT and d_4-SP TpT (1 mM total concentration) was incubated with enzyme for various times. The reaction was quenched by addition of HCl, the amount of TpT formed in the sample was determined by HPLC, and the deuterium content of the resulting TpT was subsequently determined by ESI-MS spectrometry using the Agilent 6520 Accurate-Mass Q-TOF LC/MS spectrometer. The data was acquired via Agilent MassHunter Workstation Data Acquisition (B.03.00) and analyzed via Qualitative Analysis of MassHunter Acquisition Data (B.03.00) software. As shown below,

$$v = k_{cat}/K_m[E][S] \qquad \text{Thus, } \frac{v_{\text{SP TpT}}}{v_{d4\text{-SP TpT}}} = \frac{(k_{cat}/K_m)_{\text{SP TpT}}[E][\text{SP TpT}]}{(k_{cat}/K_m)_{d4\text{-SP TpT}}[E][d_4\text{-SP TpT}]}$$

$$\text{As } \frac{[\text{SP TpT}]}{[d_4\text{-SP TpT}]} = 1, \qquad \frac{(V_{max}/K_m)_{\text{SP TpT}}}{(V_{max}/K_m)_{d4\text{-SP TpT}}} == \frac{v_{\text{SP TpT}}}{v_{d4\text{-SP TpT}}}$$

Therefore, the $^{D}(V/K)$ KIE is reflected by the ratio between the two reaction rates when the concentrations of SP TpT and d_4-SP TpT are equal (t = 0).

Due to the KIE, as the reaction progresses, the SP TpT and d_4-SP TpT concentrations are no longer the same. In our experiments the KIEs at varying time points were measured at relatively low extents of reaction of between 1% and 10%. Under these conditions the isotopic composition of the SPs varies approximately linearly with the extent of reaction. The $^{D}(V/K)$ KIE was therefore calculated by linear extrapolation of the measured KIEs to zero extent of reaction when the concentrations of SP TpT and d_4-SP TpT were equal (86). The V_{max} KIE determined is different from the

corresponding $^{D}(V/K)$ KIE for the SPL enzymes studied, suggesting that although hydrogen abstraction from SP is a kinetically significant step, it is not fully rate-determining.

3.3 Results

The crystal structure of SPL from *Geobacillus thermodenitrificans* [PDB ID: 4FHD] was provided by Dr. Alhona Benjdia and Professor Ilme Schlichting of the Max Panck Institute for Medical Research in Heidelberg, Germany (Figure 3.1). Structural data suggests that cysteine is close to the SP substrate (48). This further confirms that $C141_{Bs}$ is the H atom donor. The crystal structure contains a SAM and a dinucleotide SP in the enzyme active site. The distance between the SP methylene carbon and the conserved cysteine ($C141_{Bs,}$ $C140_{Gt}$) was found to be 4.6 Å, and the distance between the methylene carbon and a conserved tyrosine ($Y99_{Bs}$, $Y98_{Gt}$) was found to be 4.3 Å.

A BLAST comparison (Figure 3.2) of *G. thermodenitrificans* and *B. subtilis* indicate a 72% overall sequence homology with the radical SAM binding motif conserved 100% among the species (26).

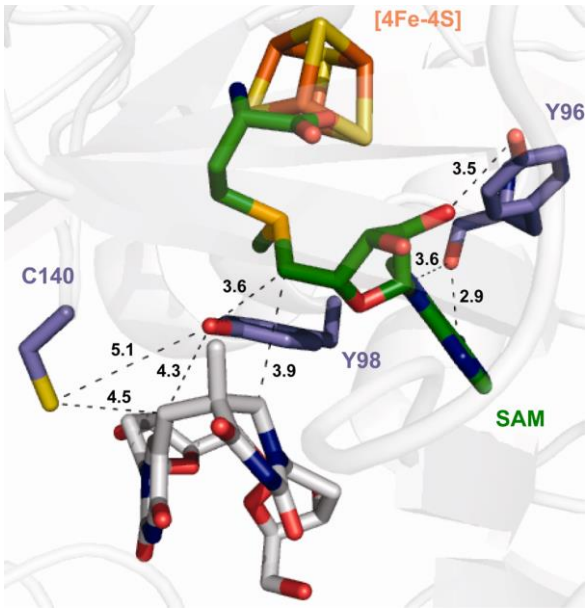

Figure 3.1: Crystal Structure of WT SPL from *Geobacillus Thermodenitrificans* (48)

Score	Expect	Method	Identities	Positives	Gaps
522 bits(1344)	0.0	Compositional matrix adjust.	243/339(72%)	282/339(83%)	0/339(0%)

```
G. thermo    PFVPKLVYFEPEALSYPLGKELYEKFTQMGIKIRETTSHNQVRGIPGETELARYRNAKST  62
             PFVP+LVY EP AL YPLG+EL +KF  MGI+IRETTSHNQVR IPG+  L +YRNAKST
B.subtilis   PFVPQLVYIEPRALEYPLGQELQDKFENMGIEIRETTSHNQVRNIPGKNHLQQYRNAKST  63

G. thermo    LVVGVRRTLKFDSSKPSAEYAIPLATGCMGHCHYCYLQTTLGSKPYIRVYVNLDDIFAQA  122
             LV+GVR+TLKFDSSKPSAEYAIP ATGCMGHCHYCYLQTT+GSKPYIR YVN+++I  QA
B.subtilis   LVIGVRKTLKFDSSKPSAEYAIPFATGCMGHCHYCYLQTTMGSKPYIRTYVNVEEILDQA  123

G. thermo    QKYINERAPEITRFEAACTSDIVGIDHLTHSLKKAIEFIGATDYGRLRFVTKYEHVDHLL  182
              KY+ ERAPE TRFEA+CTSDIVGIDHLTH+LK+AIE  G +D G+LRFVTK+ HVDHLL
B.subtilis   DKYMKERAPEFTRFEASCTSDIVGIDHLTHTLKRAIEHFGQSDLGKLRFVTKFHHVDHLL  183

G. thermo    DARHNGKTRFRFSINSRYVINHFEPGTSSFDGRLAAARKVAGAGYKLGFVVAPIYRHEGW  242
             DA+HNGKTRFRFSIN+ YVI +FEPGTS  D R+ AA KVA AGY LGF+VAPIY HEGW
B.subtilis   DAKHNGKTRFRFSINADYVIKNFEPGTSPLDKRIEAAVKVAKAGYPLGFIVAPIYIHEGW  243

G. thermo    ERGYFELFQELARQLEGMDLSDLTFELIQHRFTKPAKRVIEQRYPKTRLDLDETKRKYKW  302
             E GY  LF++L   L      D+TFELIQHRFTKPAKRVIE+ YPKT+L+LDE KR+YKW
B.subtilis   EEGYRHLFEKLDAALPQDVRHDITFELIQHRFTKPAKRVIEKNYPKTKLELDEEKRRYKW  303

G. thermo    GRYGIGKYVYRDEEAKELEDTMRRYIEQFFPGAYVQYFT  341
             GRYGIGKY+Y+ +E   L + +  YI+ FFP A ++YFT
B.subtilis   GRYGIGKYIYQKDEEHALREALESYIDTFFPNAKIEYFT  342
```

Figure 3.2: Crystal Structure Species Sequence Homology (26)

The crystal structure (Figure 3.1) identifies a conserved tyrosine, $Y98_{(Gt)}$, between the $C140_{(Gt)}$ and SAM bound in the *Gt* SPL active site, suggesting its likely involvement in the catalysis of SPL (48). Most radical SAM enzymes are known to contain an aromatic residue Φ in the vicinity of the third cysteine in the CXXXCXΦC radical SAM motif. This aromatic is suggested to maintain the position of SAM in the enzyme binding pocket through multiple interactions (48).

The conserved Φ residue ($Y96_{(Gt)}$) has a weak hydrogen bonding interaction with SAM. From this data, we believe that one or both of these tyrosine residues may play a role in an H atom relay between the thiyl radical and *5′*-dA, and are therefore involved in the SAM regeneration process.

Mutation of both tyrosines to alanines in $SPL_{(Bs)}$, allowed for the testing of these proposed roles. The Y97A-$Y99A_{(Bs)}$ double mutant maintained an intact [4Fe-4S] cluster, as confirmed by characteristic UV absorption at 420 nm and iron-sulfur content analysis. The EPR signal (provided by Joshua Telser and Stefan Stoll) of the $[4Fe\text{-}4S]^{1+}$ resulting from reduction by dithionite was similar to the wild-type (WT) enzyme. Therefore, the Y→A double mutation did not alter the stability of the iron-sulfur cluster. However, no TpT production was observed after a 3-hour reaction of the Y/A double mutant with excess SAM and dinucleotide SP TpT under reducing conditions. This inactivity demonstrates that removal of these tyrosines disrupts the interaction between the adenine ring of SAM and the phenol ring of the $Y97_{(Bs)}$, subsequently affecting SAM binding and/or reductive cleavage. Due to the conservation of the ring-ring interaction in the Y→F mutation, the Y97F-$Y99F_{(Bs)}$ double mutant should exhibit no disruption in

the SP repair reaction. However, the Y/F double mutant shows at least 100 fold slower repair reaction compared to WT $SPL_{(Bs)}$ (42).

Phenylalanine retains the aromatic ring compared to tyrosine, but does not support the radical propagation reaction due to the loss of the OH functional group (77,89). The SPL catalysis/SAM regeneration process would be changed by the Y→ F mutation should any tyrosine take part in the radical reaction.

To explore this, $Y97F_{(Bs)}$ and $Y99F_{(Bs)}$ single mutants in $SPL_{(Bs)}$ were constructed to investigate their effect on the SP repair reaction. In these single Y→F mutants, iron-sulfur content analysis and EPR spectroscopy prove that the [4Fe-4S] cluster remains intact.

Activity assays of the Y→F single mutants demonstrate that they are able to repair SP in the presence of excess dithionite and SAM, however, compared to WT enzyme (21,42) the reaction rates are 3-fold and 7-fold slower for the $Y97F_{(Bs)}$ and $Y99F_{(Bs)}$ mutants respectively, but are comparable to the rate of the $C141A_{(Bs)}$ mutant (42). Linear repair activity was observed for the first 2~5 turnovers for the WT $SPL_{(Bs)}$, $C141A_{(Bs)}$, and $Y97F_{(Bs)}$ mutants under saturating substrate conditions (30-fold of enzyme concentration). Linearity was lost in subsequent turnovers, possibly due to enzyme inactivation. Additionally, no burst kinetics was observed. In the $Y99F_{(Bs)}$ mutant repair reaction, the first turnover resulted in the fastest reaction, after which the reaction slowed down. Given the low activity of this mutant, it is difficult to determine whether the reduction in the repair rate is due to inactivation of the enzyme, or pre-steady state kinetics.

In all of the above mentioned reactions, the use of d_4-SP TpT (which has the H_{6proR} position deuterated) as a substrate, caused a decrease in the repair rate. A comparison of the initial reaction rates using the unlabeled SP and the d_4-SP TpT as substrate allows for the determination of the traditional V_{max} KIE (90). Due to the brief "steady state" for these enzyme reactions, all V_{max} KIEs were established within the first two enzyme turnovers, with the exception of $Y99F_{(Bs)}$ which was determined within the first turnover, hence we term the derived V_{max} KIEs apparent KIEs. Using mass spectroscopy, the ratio of TpT and d_3-TpT (the abstracted deuterium is washed out during catalysis) allows for the determination of the V_{max}/K_m KIE, which is termed competitive KIE.

According to theoretical calculations, both H atom abstraction steps associated with *5'*-dA (*5'*-dA formation and *5'*-dA• regeneration) in the WT SPL reaction have high energy barriers (60,91). Of the two abstraction steps, it is more difficult to take an H atom from *5'*-dA, which indicates that *5'*-dA• regeneration is more likely the rate limiting step. All previous steps are in the "rate determining zone" (37) and contribute to the rate determination process, including the H atom abstraction from SP to form *5'*-dA. As such, subsequent catalytic steps could weaken the intrinsic deuterium isotope effect associated with H-abstraction from the d_4-SP TpT. These theoretical computations imply that SAM is regenerated after each catalytic cycle (60,91), as shown in previous experimental findings that used SP containing plasmid DNA, one molecule of SAM supported > 500 turnovers (32). However one SAM molecule supports only 1.5 turnovers in our WT $SPL_{(Bs)}$, reaction with dinucleotide SP TpT as the substrate. This may

be partially contributed to the weak affinity of our substrate to the enzyme (41). It is suggested then, that during SPL catalysis, approximately two thirds of the formed *5'*-dA and methionine molecules exchange with the excess of SAM from the reaction environment. No data is currently available on the rate of this exchange step, however, the fact that the competitive KIE (3.4 ± 0.3) is higher than the apparent KIE (2.8 ± 0.3) for WT $SPL_{(Bs)}$, is an indication that SAM binding or product releasing steps are also involved in the rate limiting process (71). The observed reaction rates are the average of two reactions, one of these being SAM exchange with *5'*-dA and the other involving SAM regeneration. Due to this, these KIE numbers likely do not represent the true V_{max} and V_{max}/K_m KIEs that would result from SP containing oligomeric DNA. The complexity of the reaction process in this system makes systematic data analysis using mathematical models difficult to perform, however important mechanistic insight can be gathered from these KIE studies.

The reaction of $C141A_{(Bs)}$ mutant was also investigated, and demonstrated a reduced apparent KIE of 1.7 ± 0.02 and competitive KIE of 3.0 ± 0.02 when compared to WT SPL. The reduction in both KIEs can be attributed to a slower radical quenching step caused by the removal of the intrinsic H-atom donor on the protein (41). Also, SAM regeneration no longer takes place due to the disruption of the putative catalytic chain, and all formed *5'*-dA must be exchanged by SAM at the end of a turnover, which is in contradiction to the two thirds exchange ratio observed in WT enzyme. This apparent change in the reaction energy profile elicited by a slow exchange process between the *5'*-dA and SAM also contributes to the reduced KIEs observed in the $C141A_{(Bs)}$ mutant.

Otherwise the competitive KIEs for WT $SPL_{(Bs)}$, and $C141A_{(Bs)}$ mutant are both larger than their respective apparent KIEs, indicating that the SAM binding/*5'*-dA releasing processes are similar in these proteins.

Looking at the crystal structure (Figure 3.1), the [4Fe-4S] cluster in SPL hinders $Y96_{(Gt)}$ ($Y97_{(Bs)}$) from participating directly in the radical transfer processes via ligation to C98, the third cysteine in the radical SAM motif. $Y97F_{(Bs)}$ is identified in the crystal structure as the Φ residue in the radical SAM motif (48), this indicates a possible structural role in the correct orientation of SAM as well as subsequent *5'*-dA/*5'*-dA• intermediates to ensure efficient catalysis. This structural function can be mimicked by phenylalanine, in fact, tyrosine, phenylalanine, histidine, and tryptophan have all been found to act as the Φ residue in other radical SAM enzymes (93,94). This makes the >3-fold rate reduction observed in the $Y97F_{(Bs)}$ all the more perplexing. Additionally, the apparent KIE was 16 ± 4.5 and the competitive KIE was 11.5 ± 1.5 for $Y97F_{(Bs)}$, which is substantially larger than the respective KIEs exhibited in WT SPL. A possible explanation for these observations may be that the Y→F mutation alters the interaction of the $Y97_{(Bs)}$ residue with SAM, specifically in the loss of the –OH functional group in $Y97F_{(Bs)}$ and the 2'OH at the SAM ribose. These results could also indicate that $Y97_{(Bs)}$ is involved in another capacity in enzyme catalysis, not only in SAM binding. It also may be that $Y97_{(Bs)}$ is not a direct component of the HAT chain.

Kinetic data confirms that another residue $Y98_{(Gt)}$ (equivalent to $Y99_{(Bs)}$) may be a direct component of the HAT chain. This is also indicated by structural data of SPL. The mutant $Y99F_{(Bs)}$ results in a 7-fold reduction in the catalytic rate. The apparent KIE of

$Y99F_{(Bs)}$ was determined to be 10 ±1 and the competitive KIE was 9 ± 1, both of which are comparable to the KIEs demonstrated by the $Y97F_{(Bs)}$ mutant, but also greatly increased compared to WT SPL and the $C141A_{(Bs)}$ mutant. These inflated KIEs indicate that hydrogen tunneling is possible in this HAT step (92). It would appear that the SAM binding/*5'*-dA releasing steps are disrupted by the Y→F mutation, as indicated by the competitive KIEs being lower than the apparent KIEs in both $Y97F_{(Bs)}$ and $Y99F_{(Bs)}$ reactions, which is opposite to the trend observed in WT $SPL_{(Bs)}$, and $C141A_{(Bs)}$.

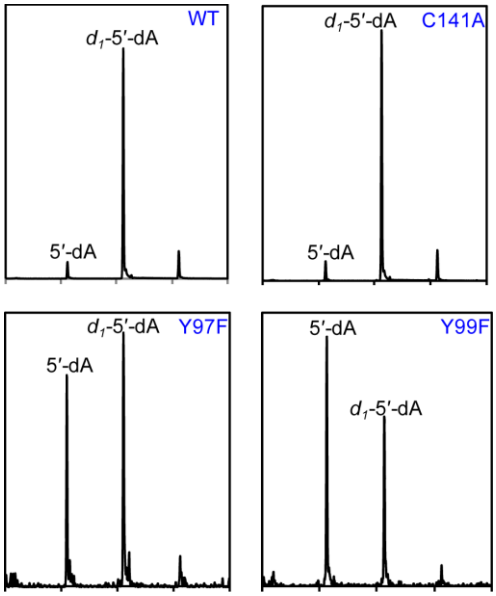

Figure 3.3: MS Analysis of *5'*-dA (42).
Mass spectrometry analysis of *5'*-dA isolated from *Bs* SPL reactions conducted with d_4-SP TpT as substrate. d_1-*5'*-dA forms via abstraction of a H atom from d_4-SP TpT, and the unlabeled *5'*-dA forms via uncoupled SAM cleavage.

The high KIEs exhibited by these Y/F mutants are supplemented by an increase in uncoupled SAM cleavage reactions. The small amount of unlabeled 5′-dA observed

(Figure 3.3) indicates that ~10% of uncoupled SAM cleavage resulted when d_4-SP was used as substrate in both WT $SPL_{(Bs)}$ and $C141A_{(Bs)}$ mutant reactions.

Contrarily, $Y97F_{(Bs)}$, and $Y99F_{(Bs)}$ demonstrated ~ 5-fold increase in the production of unlabeled *5'*-dA, showing a yield similar to that of d_1-*5'*-dA , which is the product of the H atom abstraction from d_4-SP. The high isotope effect seen in both mutants suggests that deuterium abstraction by *5'*-dA• becomes unfavorable. Consequently, ~ 50% of the *5'*-dA• is quenched by reductants from the environment.

The enhanced uncoupled SAM cleavage reaction in these Y/F mutants indicates that the protein local conformation is essential for an efficient SPL catalysis. Cleavage of the strong C5'-S bond in SAM is assisted by the protein network to rapidly quench the resulting *5'*-dA•, enabling a quick and efficient SP repair reaction.

To ensure that the $Y99F_{(Bs)}$ mutation did not alter the structure of the protein, the crystal structure of the corresponding $Y98F_{(Gt)}$ mutant in *Gt* SPL was determined to a resolution of 2.3Å. When compared to the structure of WT enzyme, the $Y98F_{(Gt)}$ mutant shows structural integrity and a conserved conformation with overall r.m.s.d of 0.15Å for the superimposed protein backbone, particularly well-matched are the phenylalanine and the WT tyrosine (Figure 3.4). The active site of the $Y98F_{(Gt)}$ mutant shows that its overall architecture as well as the interactions between the protein and SAM are highly similar to the WT enzyme (48). The WT $SPL_{(Gt)}$ and $Y98F_{(Gt)}$ mutant repair SP TpT at reaction rates of 0.32 and 0.04 min^{-1} respectively, both of which are comparable to those observed by the equivalent *Bs* enzymes . Additionally, these *Gt* enzymes demonstrate identical apparent KIEs to their *Bs* equivalents. Considering the ~

80% sequence identity between these two enzymes, we conclude that the structural information obtained for *Gt* SPL also reflects the *Bs* enzyme.

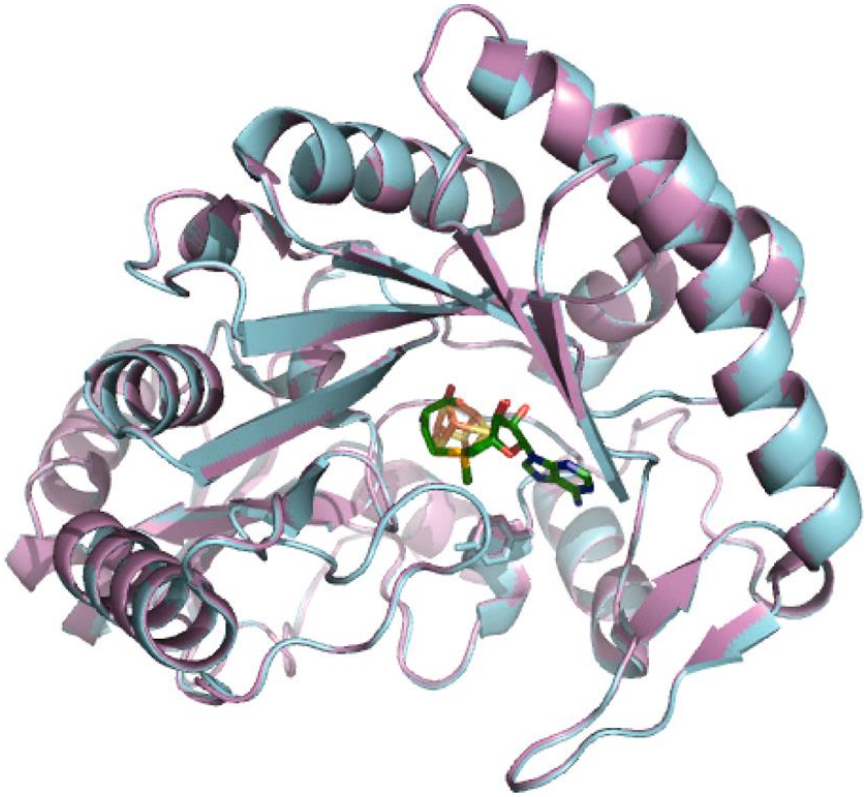

Figure 3.4: Secondary Structure of WT SPL (42).
Secondary structure of substrate free WT $SPL_{(Gt)}$ (cyan) and the Y98F(Gt) mutant [purple, equivalent to the Y99F(Bs) mutant Protein Data Bank entry 4K9R]. The superposition of both structures was performed with Coot using the SSM program and all residues.65 The iron–sulfur cluster is colored orange (Fe) and yellow (S). SAM is colored by atom type (green for C, blue for N, red for O, and yellow for S). Y98 in the WT SPL(Gt) and F98 in the Y98F(Gt) mutant are depicted in stick format.

Enzyme kinetic studies, as well as the structural data imply that the two tyrosine residues are involved in the SPL catalytic cycle. They must play a role in the radical relay chain downstream of $C141_{(Bs)}$, the intrinsic H atom donor. The crystal structure of $SPL_{(Gt)}$

supports the functional assignment of $Y99_{(Bs)}$ to be directly involved in the radical transfer to facilitate SAM regeneration (Figure 3.5).

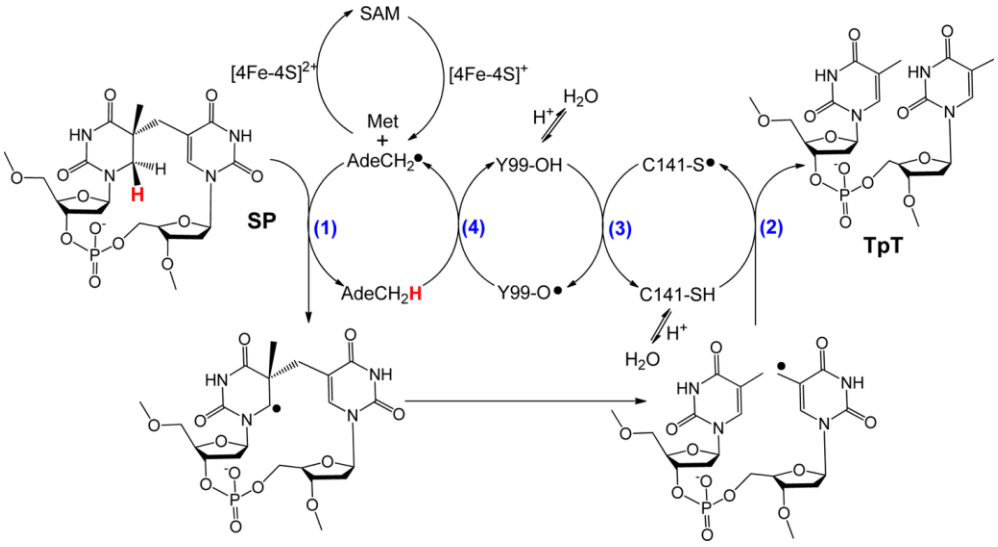

Figure 3.5: Hypothetic SPL Reaction Mechanism (42).
Hypothesized reaction mechanism for SPL (the residues are numbered according to the protein sequence in *Bs* SPL). This mechanism implies that SPL uses a minimum of four H atom transfer processes (blue number labels) in each catalytic cycle. One of the four processes occurs between a tyrosine and a cysteine, suggesting that SPL uses a novel HAT pathway for SAM regeneration. The role of $Y97F_{(Bs)}$ still needs to be determined and is therefore not shown here.

$Y98_{(Gt)}$ (equivalent of $Y99_{(Bs)}$) is situated between C140 and SAM; its hydroxyl group is 5.1 Å away from the SH moiety of C140, and 3.6 Å away from the methylene carbon of SAM (Figure 3.1). This close proximity to the 5'-dA moiety makes it well positioned for the radical relay process to mediate SAM regeneration. Following the SAM cleavage reaction $Y99_{(Bs)}$ also helps stabilize the transient protein conformation, enabling a concerted enzymatic reaction. It is likely that a conformational change occurs in the protein after cleavage of the C5'-S bond prior to the 5'-dA• abstraction of

the H_{6proR} atom to initiate the SP repair process. Enhancement of uncoupled SAM cleavage (Figure 3.3)indicates that this conformational change is disrupted in the $Y99F_{(Bs)}$ mutant, and is also expected for the $Y97F_{(Bs)}$ mutant reaction.

The tightly coupled radical relay mechanism is consistent with our experimental finding that no organic radical intermediate was observed by EPR spectroscopy in the "steady state" of the WT $SPL_{(Bs)}$ catalyzed SP TpT repair reaction. This suggests these putative radical intermediates in Figure 3.3 exist as transient species. SPL catalysis likely occurs in a concerted fashion: once the radical intermediate is generated via SAM reductive cleavage, it will be passed quickly through the catalytic chain until the end of the reaction. This process is facilitated by transient protein conformational changes, preventing any of the intermediates from accumulating.

The observed TpT/*5'*-dA ratios in the $SPL_{(Bs)}$ reactions are not entirely supportive of our proposition that SAM is regenerated after each catalytic cycle. Studies indicate an ~1:1 observed ratio between SP TpT consumed and *5'*-dA formed in both $C141A_{(Bs)}$ (41) and $Y99F_{(Bs)}$ reactions which appears to confirm that these residues are involved in the HAT chain for SAM regeneration, however in both WT $SPL_{(Bs)}$ (42) and $Y97F_{(Bs)}$ mutant reactions, the ratio is ~1.5:1 indicating that only one third of SAM is regenerated in these reactions. This discrepancy may be due to a much weaker binding affinity of the dinucleotide SP TpT compared to SP containing duplex DNA. DNA foot-printing studies indicate that $SPL_{(Bs)}$ covers a region of at least 9-bp surrounding SP in which negatively charged phosphodiester moieties enhance the binding interaction of SPL (94). DNA photolyase, which repairs the cyclobutane dimer, gives a comparable example in

its recognition of 6-bp surrounding the dimer. A 10^4-fold decrease in binding affinity was observed for binding of the dinucleotide thymine dimer to photolyase compared to binding with dimer containing oligonucleotide (95). This demonstrates that substrate binding to enzyme is severely weakened by the loss of electrostatic interactions resulting from the removal of phosphodiester moieties on either side of the dimer. Considering that $SPL_{(Bs)}$ recognizes 3 more phosphodiester groups than photolyase, the binding affinity of dinucleotide SP TpT is likely to be much weaker than that of SP containing duplex oligonucleotide. Therefore, in order to fully establish the mechanism outlined in Figure 6, d_4-SP containing oligonucleotides will be necessary to re-examine the KIEs reported here. Such experiments are not trivial considering the synthetic challenge to prepare enough deuterium labeled SP containing oligomers. However, the substrates used in these studies provide strong support for the proposed mechanism in their demonstration of the obvious differences in the reaction rates as well as the apparent and competitive KIEs between the WT and mutant SPL proteins. Additionally, the observation of similar SAM regeneration patterns in $Y97F_{(Bs)}$ mutant and WT $SPL_{(Bs)}$ supports our hypothesis that $Y97_{(Bs)}$ may not be a direct component of the HAT pathway. In conclusion, our report strongly implicates SPL to be the first member of the radical SAM superfamily to possibly bear a HAT chain. This transfer chain is likely to be essential for SAM regeneration in SPL catalysis. Currently, only SPL and lysine-2,3-aminomutase have been shown to use SAM catalytically (96,97). However, considering the large number of radical SAM enzymes discovered to date (more than 44,000 (80)) a catalytic role of SAM can be expected among additional members of this superfamily. Our studies

thus provide much-needed insight in understanding the SAM regeneration process not only in SPL, but potentially to other radical SAM enzymes.

3.4 Acknowledgements

The research discussed in this chapter was a collaborative effort of many individuals to whom credit must be given. Special thanks to Linlin Yang, Alhosna Benjdia, Gengjie Lin, Joshua Telser, Stefan Stoll, Ilme Schlichting and Lei Li for their contributions and dedication to this project and publication.

"A Radical Transfer Pathway in Spore Photoproduct Lyase" Biochemistry. April 15, 2013. 3041-3050.

CHAPTER 4. GLYCINE 168 RESIDUE OF SPL FROM *B. SUBTILIS*

4.1 Introduction

In genetic studies of *B. subtilis* SPL, Cavazos and Nicholson (98) observed three recombinant classes in a transformational cross between wild-type *spl* gene and a mutant *spl-1* of *B. subtilis*. Type I recombinant class spores exhibit UV resistance, and Type III is UV sensitive. The finding of a third class of spores resulting from these recombination studies led to an interest in the glycine 168 residue of *B. subtilis* SPL. This class (Type II) yields spores which, following UV irradiation, exhibit slower germination kinetics. It was deduced that two mutations exist in the *spl-1* allele, an arginine replaced glycine 168 (G168R), and aspartic acid took the place of glycine 242 (G242D). Furthermore, G168R had a greater contribution to the *spl-1* phenotype than G242D. Hence to conclude my studies of SPL, purification and full characterization was performed on G168A and G168R mutant SPL to determine the effect of this genetic mutation on the ability of SPL to repair the UV damage product 5-thyminyl-5,6-dihydrothymine, or SP. Mutation of this glycine to alanine demonstrated little disruption in the SP repair process.

4.2 Experimental Methods

4.2.1 Expression and Purification of SPL G168A Mutant

The protein purification as well as the enzyme reactions were carried out under an inert atmosphere using a Coylab anaerobic chamber (Grass Lake, MI) with the H_2 concentration around 3%. Both the WT SPL and the G168A mutant were expressed in LB (Luria Bertani) medium containing the antibiotics ampicillin (100 μg/mL) and kanamycin (25 μg/mL). The harvested cells were re-suspended in binding buffer containing 25 mM Tris, 250 mM NaCl and 10% glycerol (pH 7.0) supplemented by 5 mM 2-mercaptoethanol and 1 mM PMSF, and were disrupted by sonication. Following ultracentrifugation the supernatant was loaded on a Ni-NTA (Qiagen) column equilibrated with binding buffer. Proceeding steps were carried out in the Coylab anaerobic chamber. The bound protein was washed with binding buffer containing 20 mM imidazole for 10 column volumes. The protein was then eluted with 500 mM imidazole. Further purification was achieved by ion exchange chromatography using the SP Sepharose fast flow ion exchange resin (GE Healthcare Life Sciences, Piscataway, NJ). The bound protein was washed using a buffer containing 25 mM Tris, 250 mM NaCl and 10% glycerol (pH 7.0) for 10 column volumes. The protein was then eluted using the same buffer containing 500 mM NaCl instead. The resulting protein was diluted by 2-fold to reduce the salt concentration to 250 mM and saved for activity studies. In a separate purification process, the protein was dialyzed in phosphate buffer containing 25 mM sodium phosphate, 250 mM NaCl and 10% glycerol (pH 7.0).

Purification of the G168R mutant was attempted using the above method, however this proved to be inefficient to achieve the >95% protein purity seen when employed with WT SPL or other mutants. Procedural modifications were explored as detailed in later sections.

4.2.2 Small Scale Purification of SPL G168R Mutant

E. coli BL21 (DE3) cells containing the vector for expression of G168R as well as the pDB1282 vector were plated on an LB agar Amp+ Kan+ plate and incubated overnight at 37°C. A single colony of cells was placed in 1.5 mL of LB XYT broth containing 100 µg/mL ampicillin and 25 µg/mL kanamycin and allowed to grow to OD 600 at which time 15 mL of broth was added and the cells were transferred to a 150 mL Erlenmeyer flask on the shaker at 37°C. After 8 hours, expression of G168R was induced by the addition of 0.5 mM IPTG and 0.004 mg of $Fe(NH_4)_2(SO_4)_2$. Temperature was reduced to 16°C and cells incubated on shaker overnight. The following morning, cells were placed in a centrifuge tube and spun at 5500 rpm for 12 minutes at 4°C (Eppendorf Centrifuge 5804R). The pelleted cells were kept on ice for the remainder of the purification process. All buffers were purged with argon and also kept on ice. Cells were resuspended in 0.5 mL binding buffer containing 25 mM Tris, 250 mM NaCl and 10% glycerol (pH 7.5) supplemented with 5 mM 2-mercaptoethanol and 1 mM PMSF. Sonication was carried out (t=10, amplitude=40%, pulse 2:8), followed by centrifugation at 5500 rpm for 7 minutes at 4°C. Supernatant was recovered. The proceeding steps were all carried out at 4°.

Small scale column was prepared by placing 300 µL of Ni-NTA beads into a microcentrifuge tube, beads were allowed to settle and storage liquid was removed. To the drained beads, protein containing supernatant and a stir bar were added. This mixture was stirred for 10 minutes to allow his-tags on protein to bind with the beads. The mixture was then centrifuged (Eppendorf 5424) at 200 rpm for 3 minutes and the supernatant was removed (labeled binding flow through). Wash buffer containing 25 mM Tris, 250 mM NaCl, 10% glycerol and 20 mM Imidazole was added in 600µL aliquots, the solution stirred to mix thoroughly and then centrifuged at 2000rpm for 4 minutes. The beads were washed multiple times (3-5), each time removing the supernatant (labeled wash 1, 2 etc.). The protein was then eluted with buffer (similar to the wash buffer but containing 250 mM imidazole instead) in 200µL aliquots (repeated twice), centrifuged as before and the eluates collected (labeled elution 1, 2). All samples were placed in the -20°C freezer until needed for further analysis. Modifications to this procedure included; variations in NaCl concentration (350 mM vs. 250 mM), varying imidazole concentrations during washing steps (10 mM, 15 mM, and 20 mM), variations in number of wash steps, and the addition of either 1% Triton, or 8 M Urea.

4.2.3 Iron and Sulfur Content Analysis

The quantification of iron in SPL from *B. subtilis* was determined by the method of Fish (46) with a few modifications to the original procedure. In the iron releasing step, 3% nitric acid was mixed with equal volumes of 4.5% (w/v) $KMnO_4$, rather than 1.2 M HCl for Reagent A. Additionally, the samples and standards were brought to volume

(1mL) with 3% nitric acid instead of DI H_2O. The reducing, iron-chelating reagent; Reagent B was made by reducing the amount of ascorbic acid from 8.8 g to 8.25 g/25 ml reagent B, to keep from precipitating out excess ascorbic acid. All other components of Reagent B were kept in accordance with the original procedure.

Reagents: Iron standard stock 200 ppm (Fisher Scientific), 3% nitric acid, 4.5% (w/v) $KMnO_4$, Reagent B: 8.25 g ascorbic acid, 9.7 g ammonium acetate, 80 mg Ferrozine, and 80 mg neocuproine brought to final volume 25 mL with DI H_2O. Standards were made by diluting the Iron Standard Stock 10-fold and brought to final volume 1 mL with 3% nitric acid. Protein samples were also prepared with 3% nitric acid. Equal volumes of 3% nitric acid and 4.5% $KMnO_4$ were mixed in the hood and 500 µL was quickly added to each standard and sample. The samples were vortexed and placed in a heating block at 60°C for 2 hours. After the samples had cooled to room temperature, 100 µL of Reagent B was added (one sample at a time) and thoroughly mixed. The reaction was allowed to proceed uninterrupted for 30 minutes before the absorbance of each sample was measured at 562 nm. From the linear relationship of the iron standards, the quantity of Fe (µg) detected in the protein samples was determined. (See Figure 4.1)

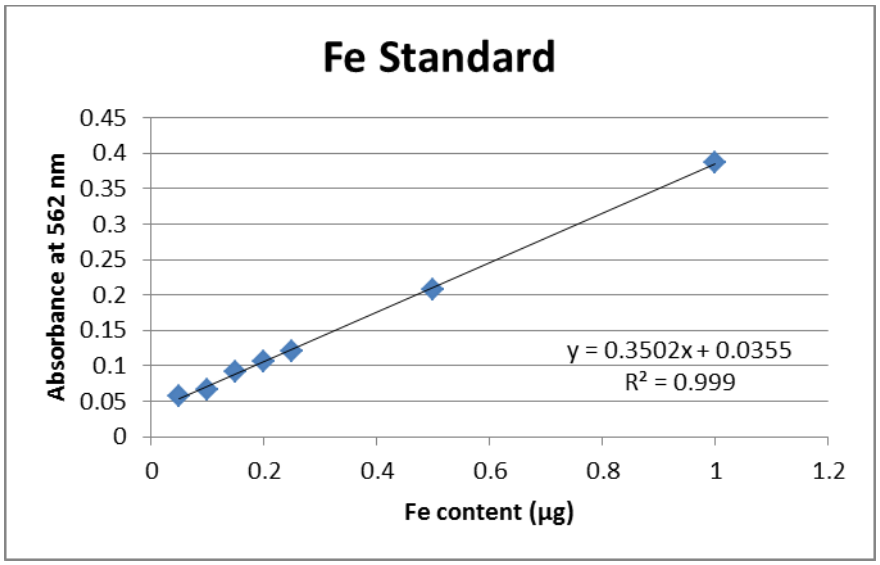

Figure 4.1: Fe Standard Curve
Fe Standard Curve; determined by the absorbance at 562 nm, indicating the quantity of colorimetric Fe-Ferrozine$_3$ complex present.

Sulfur content was determined using the method described by Bienert (47). The following reagents were made just prior to performing assays; 0.01 M Na_2S in 0.1 M NaOH (sulfur standards), 10% zinc acetate (diluted to 1% when used), 0.1% DMPD, and 23 mM $FeCl_3$ in 1.2 M HCl. Sulfur samples were made at 1, 1.5, 2, 2.5, and 3 nmol concentrations by adding the appropriate volume of Na_2S and DI water to a final volume of 100 µL in a microcentrifuge tube containing a miniature stir bar. To each sample, 300 µL of 1% zinc acetate quickly followed by 15 µL of 12% NaOH were added and stirred. The samples were allowed to incubate for a period of 1 hour before the addition of 75 µL 0.1% DMPD to the bottom layer of the resulting solution which was then stirred gently until the vortex reached the top 2 mm of solution. 75 µL of 23 mM $FeCl_3$ was added and the solutions stirred until homogeneous.

After a 30 minute incubation period the samples were centrifuged and then analyzed for their absorbance at 670, 710, and 750 nm on the UV-Vis spectrometer. As with the Fe content assays, a standard curve was created to determine the sulfur content of each protein sample.

4.2.4 Protein Concentration and Purity Assays

Protein concentrations were determined based on the absorption of aromatic residues at 280 nm with the addition of 6M guanidine hydrochloride using the method described by Gill and Von Hippel using the value of 37460 for the molar absorptivity coefficient for SPL (45). Absorbance was measured using Thermo Scientific NanoDrop 2000 UV-Vis Spectrophotometer.

Protein purity was observed via SDS-PAGE, as well as ESI-MS analysis by deconvolution on the Agilent 6520 Accurate-Mass QTOF LC/MS spectrometer. Purified protein samples were treated on C-18 spin columns to remove components of buffer which may affect ionization by electrospray. Using Agilent MassHunter Workstation Data Acquisition (B.03.00), initial mass data was collected with; gradient- 80% A/20% B (H_2O: 0.1% formic acid, ACN: 0.1% formic acid), flow rate- 100 µL/min, injection volume- 1 µL, dry gas- 8 L/min, nebulizer- 30 psig, gas temp- 325°C, instrument state- 1700 m/z, high resolution, fragmentor- 200 V, VCAP- 4000 V. Data analysis via deconvolution was carried out using Qualitative Analysis of MassHunter Acquisition Data (B.03.00) software.

4.2.5 Protein Analysis by Size Exclusion Chromatography

Chromatography was performed at room temperature on Shimadzu HPLC using a Shodex SB-804 HQ size exclusion column equilibrated with buffer containing 25 mM Tris and 250 mM NaCl. A continuous gradient of this buffer was used at 0.750 mL/min flow rate for 30 minutes. Standards (Shodex) were used for comparison of the peaks observed by the 50 µL samples of protein analyzed, including SPL WT, G168A, and G168R.

Enzyme activity reactions, V_{max} KIE, and V_{max}/K_m KIE analysis were all carried out on G168A and G168R using the methods previously described in Chapter 3 of this thesis.

4.3 Results and Discussion

4.3.1 Analysis of SPL G168A Mutant

Investigation into the possible contribution that glycine 168 of *B. subtilis* SPL had on the effectiveness of the enzyme catalysis began with the expression and purification of G168A and G168R mutant SPL.

Purified G168A mutant protein is subjected to ESI-MS analysis by deconvolution on the Agilent 6520 Accurate-Mass QTOF LC/MS spectrometer. The average molecular weight of deconvoluted protein, as calculated by MassHunter Qualitative Analysis software based on the protein sequence, was 43514 Da for G168A. Figure 4.2 identifies the deconvolution spectra for G168A which suggests >90% purity and correct mass for the G168A mutant SPL.

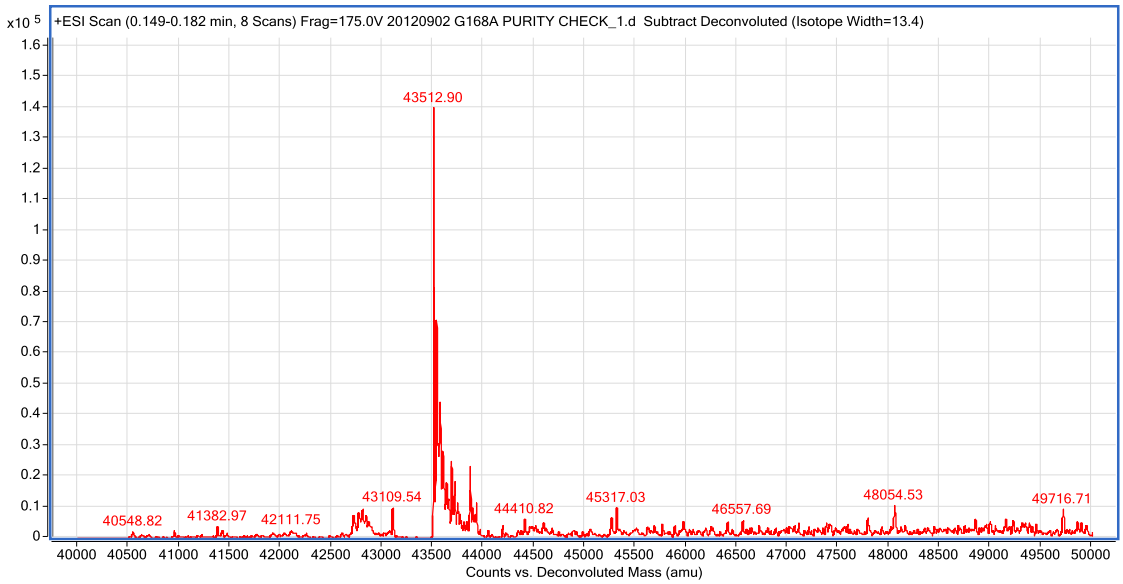

Figure 4.2: Deconvolution for G168A
Deconvolution spectra for G168A SPL purity confirmation.

Purification of G168A mutant SPL indicated an intact [4Fe-4S] cluster as identified by the dark-brown band marking the elution from the ion exchange column. Confirmation was provided by the presence of the characteristic UV absorption band at 420 nm. Iron and sulfur content assays suggested that each molecule of purified protein contained 3.58 ± 0.01 Fe and 2.7 S.

Kinetic analysis suggests that G168A repairs SP at a rate of 1.2 ±0.3 min^{-1} which was comparable to the WT SPL rate of 1.03 min^{-1} determined in the same study. This evidence shows that no disruption in the repair reaction is observed in the G→A mutation. The competitive KIEs for WT and G168A SPL were nearly identical, exhibiting 4.8 ± 0.4 and 4.9 ± 0.6 respectively. Looking at the apparent KIE however, the decreased KIE of G168A was 1.87 ± 0.08 vs. the 2.37 ± 0.3 apparent KIE of WT SPL. This may indicate that the SAM binding or product release step may be slightly delayed by the

mutation of glycine to alanine, but this structural variation is not significantly enough to affect the ability of G168A to perform repair of SP.

4.3.2 Analysis of SPL G168R Mutant

Ideally, the changes in these reported kinetic values of G168A would have been compared to those demonstrated by G168R, however activity studies were interrupted by difficulties in obtaining a purified G168R SPL protein. Following is a discussion about those purification procedures, outcomes observed and method modifications tested.

Results indicate that the purification process for G168R mutant SPL was unsuccessful for isolating functional protein. As shown in Figure 4.3, there are several proteins identified by convolution, and the major peak which we expect would correlate with G168R does not match the mass predicted for the protein which is 43599 Da.

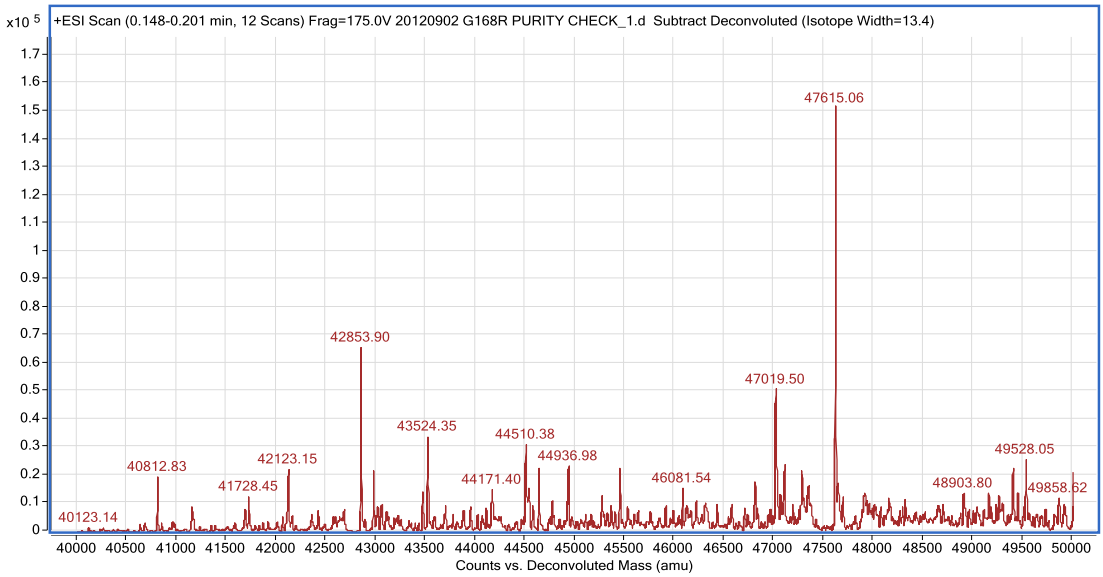

Figure 4.3: Deconvolution for G168R
Deconvolution spectra from ESI-MS for purified G168R SPL.

Analysis by SDS-PAGE (Figure 4.4) confirmed the purity results of G168A and G168R mutants that were also collected via ESI-MS.

Initial purification of G168R was carried out using only the Ni-NTA beads, as earlier purification attempts employing the use of the ion-exchange column gave visual indication of disruption to the iron-sulfur cluster (yellow bands of protein disappearing and turning clear on the column). In an attempt to remove some of the contaminating proteins, dialysis was performed on half of the resultant protein. As indicated in Figure 4.4, this additional purification step did little to eliminate the contaminants.

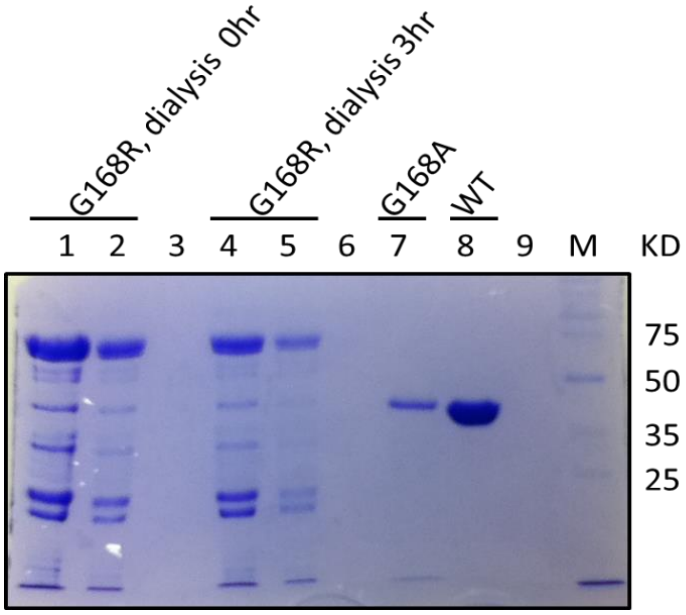

Figure 4.4: SDS-PAGE of G168A, G168R

SDS-PAGE (12% acrylamide) of purified G168A, G168R and WT SPL. Lanes 1 and 2 are purified G168R without post-purification dialysis, where lanes 4 and 5 are the same protein which underwent dialysis for 3 hours following elution from Ni-NTA column. Lane 7 identifies the purified G168A mutant SPL which corresponds with the band in lane 8 of purified SPL WT.

Experiments followed to identify which aspect of the expression and purification processes most contributed to the inability to obtain purified G168R SPL. To determine if the problem existed in the expression phase, four cell cultures were prepared by a fellow researcher, LinLin Yang. Two of the cell cultures contained pET28a expression vector, one of which harbored the G168R gene (SPL G168R + pET28a) and the other an empty vector (pET28a). The other two cell cultures expressed the pET28a vector, again with only one containing the G168R gene, though this time these cultures co-expressed plasmid pDB1282 (SPL G168R + pET28a + pDB1282, and pET28a + pDB1282). Purification and analysis by SDS-PAGE of the resulting gene products indicated that G168R was indeed being expressed; although seemingly so were several other unidentified proteins (Figure 4.5).

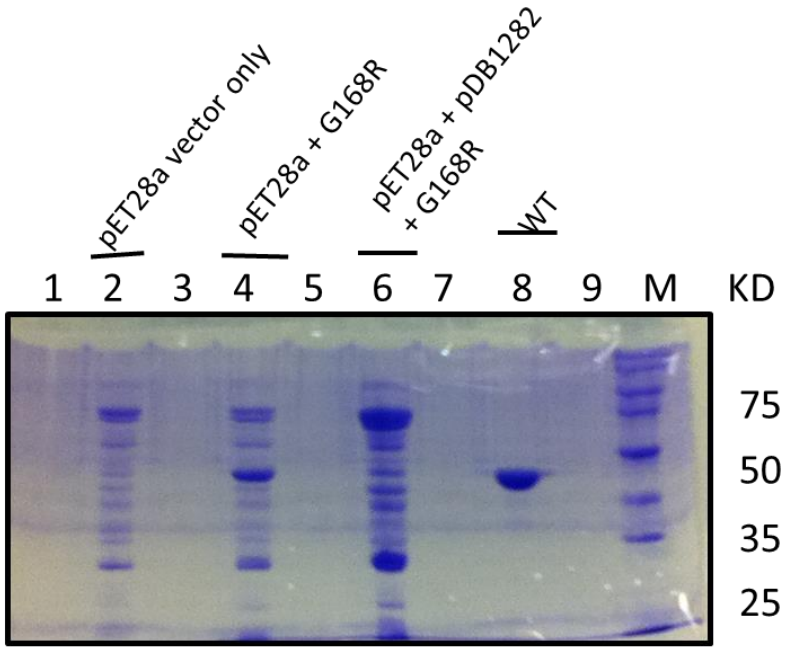

Figure 4.5: SDS-PAGE of G168R Vectors
SDS-PAGE elution fractions from vector and G168R purification.

Having concluded that expression was not the problem, I further investigated whether the formation of inclusion bodies in the steps immediately following expression could explain the lack of purified G168R SPL. Another round of purification commenced and aliquots were collected for the following fractions; whole cell in medium, cell pellet, supernatant (post pelleting), post sonic pellet, post sonic supernatant, binding flow through (after addition onto column), all wash fractions, and all elution fractions. The indication was that although a representative mass on SDS-PAGE identified some inclusion bodies in the early steps of purification, there was also protein thought to be G168R in elution fractions, although far from pure.

Several procedural modifications were attempted to isolate G168R from the contaminating proteins. Wash buffer imidazole concentrations were varied from 10-20 mM, the number of washing steps was increased from 3 to 5 washes, increasing the NaCl concentration from 250 mM to 350 mM, addition of 1% Triton, and presence of 8 M Urea were each performed (separately) to reduce the nonspecific binding of proteins to the Ni-NTA beads, hence rendering a more purified G168R mutant SPL. Unfortunately, months of investigation failed to elucidate the optimal conditions or procedural changes necessary to isolate G168R in any reproducible way. The most successful of these attempted method changes occurred with the addition of 8M Urea. Figure 4.6 illustrates the supernatant and elution fractions of G168R + pET28a in the presence of 8M urea in lanes 1 and 2 respectively. The singular band in lane 2 represents the most pure protein product obtained for G168R, however QTOF analysis identified that this was not pure G168R, and the denatured protein is rendered useless

for further kinetics studies. Lanes 4, 5, and 6 contain G168R + pET28a binding flow-through, supernatant and elution fractions purified without the addition of 8M urea. Although there are significantly fewer contaminating proteins than in previous purification attempts, isolation of G168R was not achieved.

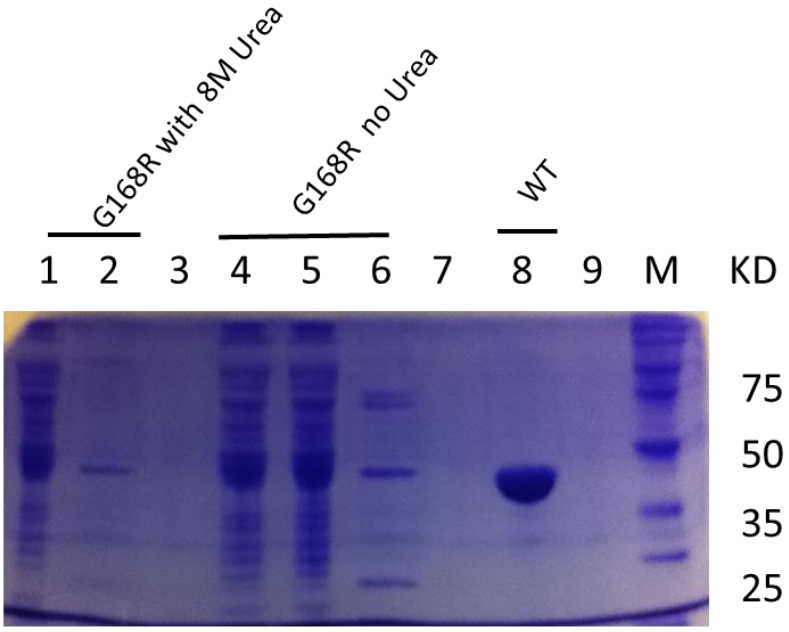

Figure 4.6: SDS-PAGE of G168R with/without Urea
SDS-PAGE of G168R mutant SPL with or without 8 M Urea. Lane 1 is the supernatant; lane 2 is the purified G168R with 8M urea. Lane 4 is the binding flow through from Ni-NTA beads, lane 5 is the G168R supernatant and lane 6 is the first elution fraction of purified G168R with no urea. Lane 8 is SPL WT, and lane 10 is the standard.

Additional assays were conducted on the elution fraction (Figure 4.6 lane 6), including activity studies, deconvolution, and trypsin digestion followed by ESI-MS analysis of resultant fragments. Activity assays did not allow for the determination of a reaction rate, as the amount of repaired SP (even after incubation for several hours) was comparable to the noise level registered on the HPLC. This seems to indicate that

should this protein be G168R, this mutation disrupts any ability of the protein to perform enzymatic catalysis in the repair of SP.

To determine if this was indeed G168R, deconvolution and trypsin digestion were done on the elution fraction containing only the 40kDa band resulting from purification with 8M urea (Figure 4.6 lane 2). Although a digestion fragment was identified by MassHunter correlating with the expected mass of the fragment containing G168R, deconvolution results could not confirm by mass that the purified protein was G168R. Interestingly, the most predominant mass found in the 40,000Da range presented in multimer fashion, with dimers and quatromers located when deconvolution was carried out in those mass ranges (Figure 4.7).

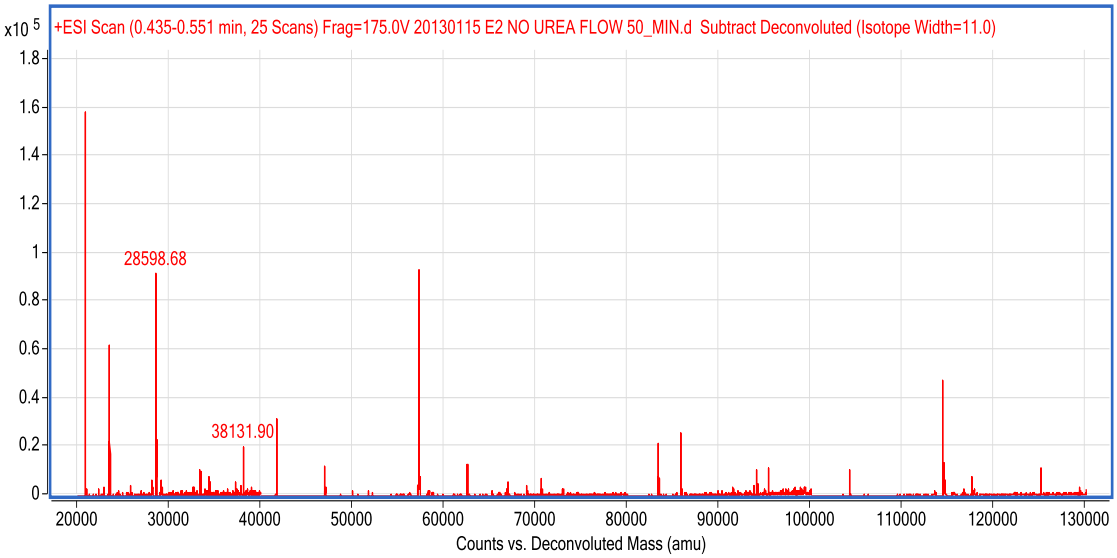

Figure 4.7: Deconvolution of Wide Mass Range for G168R
ESI-MS deconvolution spectra over wide mass range for G168R protein.

The inability to reproducibly purify G168R demanded an explanation. Taking a closer look at the crystal structure of *bacterium Geobacillus thermodenitrificans* SPL, and

the location of the glycine 168 ($G167_{(Gt)}$) may provide a simple answer. The solved crystal structure (59) was modified utilizing PyMOL ™ (Copyright 2006 Delano Scientific LLC), protein imaging software to depict the G168R mutation. This residue is quite remote from the active site (Figure 4.8) indicating that it likely does not function in any catalytic role, however the proposed disruption caused by this mutation would very likely result in a catalytically incompetent protein

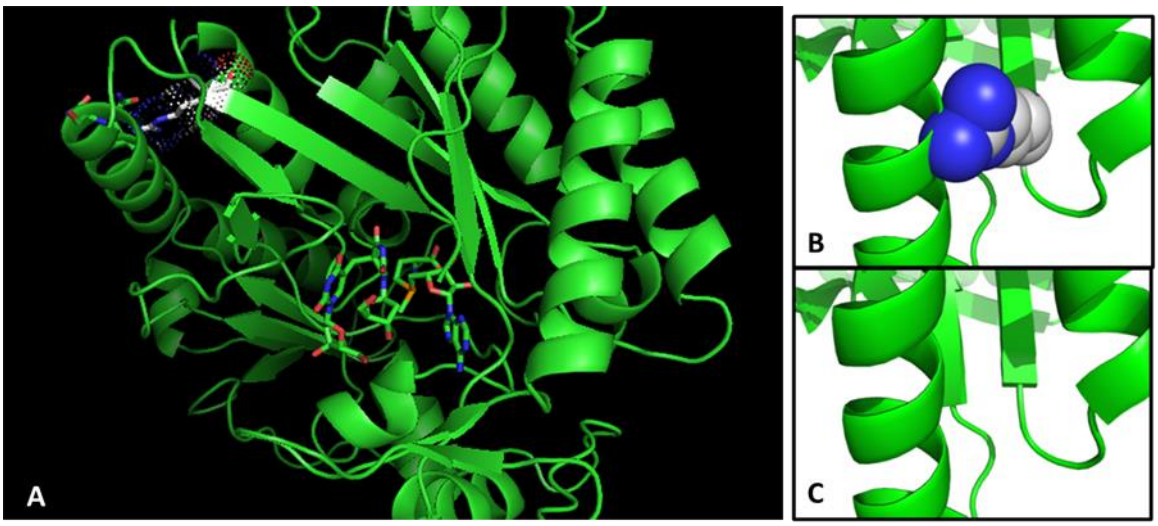

Figure 4.8: PyMOL of G168R

PyMOL representation of G168R SPL. A) G168 mutation site relative to the center active site. B) Close up of the G168R mutant site. C) Close up of the WT at G168 site.

Figure 4.8 also provides a close up of the G168R mutation (as depicted by PyMOL) and WT SPL respectively. Not only is it problematic that the glycine is situated in a location that transitions from β-barrel to α-helical motif, but the addition of such a bulky mutation causes steric hindrance with the neighboring α-helix which would certainly result in a protein incapable of folding into the proper conformation to allow enzymatic catalysis.

Representation of the electrostatic interactions introduced by the G→R mutation (Figure 4.9) may also explain the instability demonstrated by the G168R SPL during purification.

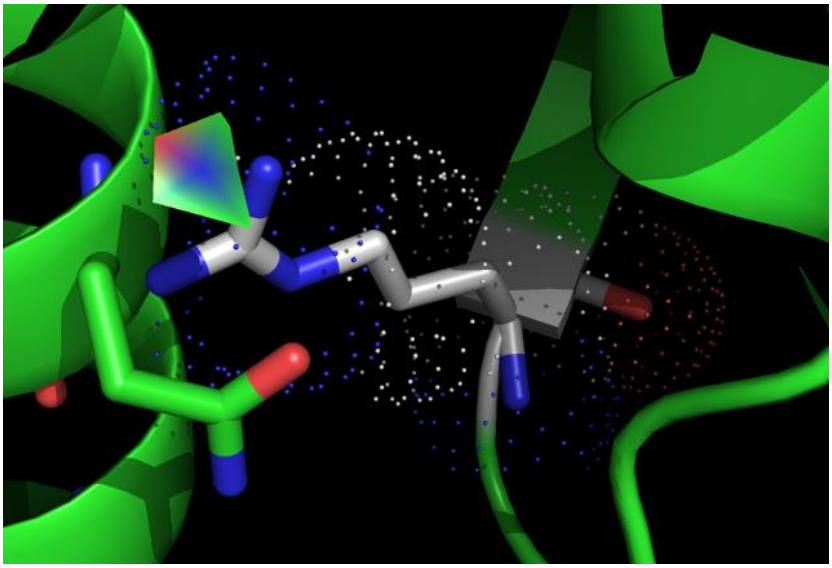

Figure 4.9: PyMOL of Electrostatics
PyMOL representation of SPL G168R mutant identifying electrostatics.

Based on the inability to isolate a solitary protein through purification, and the lack of quantifiable activity, it is therefore deduced that expression of the *spl-1* allele containing the genetic modification of G168R (alone or in addition to G242D) should render a gene product with little to no ability to perform enzymatic catalysis on the UV damage product SP.

CHAPTER 5. CONCLUSIONS AND FUTURE OUTLOOK

5.1 Conclusions of SPL Mechanistic Studies

These studies have confirmed C141 in *B, subtilis* to be the intrinsic H atom donor in the repair of SP by SPL enzymatic catalysis. The C141 can be readily alkylated by iodoacetamide proving this residue is accessible to TpT. The rate of repair of C141A mutant is 0.14 ± 0.02 min^{-1} compared to 0.41 ± 0.03 min^{-1} in WT SPL demonstrating that this mutation decreases the rate of the repair reaction 3-fold. Apparent KIE and competitive KIE are 1.7 ± 0.2 and 3.0 ± 0.3 respectively and indicate that interrupting the H atom back donation to TpT by this C→A mutation interferes with the rate limiting process in enzymatic catalysis.

Further, mutating the conserved tyrosine residue Y99 in *B. subtilis* shows a significant reduction in the rate of repair (0.06 ± 0.0005 min^{-1} in Y99F) compared to WT. A 1:1 ratio of SP repaired to *5'*-dA generated also shows that SAM regeneration is not possible in the Y99F mutant reactions. Additionally, the Y99F mutant has an apparent KIE of 10.5 ± 1 and a competitive KIE of 9 ± 1 suggesting that the rate determining step in this mutant SPL reaction may change from the *5'*-dA• regeneration (as in WT) to the initial H_{6ProR} abstraction by *5'*-dA in the initiation of SP TpT repair. These results indicate

that the H atom transfer chain to regenerate SAM for subsequent catalytic cycles is not possible in the absence of this critical Y99 residue.

Studies of the Y97F mutant also demonstrate significant inflation of the apparent KIE (16 ± 1.5) and competitive KIE (11.5 ± 1.5) suggesting that Y97 may play more than the structural role indicated by crystal structure analysis.

Although more work is needed to fully understand the mechanism of SPL enzymatic repair of SP, the research here provides strong proof that SPL utilizes a novel H atom transfer (HAT) chain to repair the UV-induced DNA damage to *B. subtilis* endospores.

5.2 Future Studies of SPL

The main limitation in this body of work is in the use of dinucleotide SP TpT as a substrate. Without interaction of the SPL and the phosphodiester backbone of DNA (as *in vivo*) the binding affinity of SPL for the substrate is weakened which could play a role in the results acquired utilizing dinucleotide SP TpT as a substrate. To improve the enzyme-substrate binding affinity further studies are being performed using SP containing duplex oligonucleotides as substrate for the SPL reactions.

Structural analysis indicate that Y97 plays a critical role in SAM binding to SPL, however, kinetic studies seem to suggest that there may be another role being performed by this residue. Additional studies are necessary to characterize the role of Y97 in the enzymatic catalysis of SPL.

Due to the stereoselectivity of the *5'*-dA• H atom abstraction from the *5'*-T to initiate SP repair, inhibition studies could be performed by introduction of a different moiety to this position on *5'*-T.

REFERENCES

REFERENCES

(1) Prescott, L. M., Harley, J. P., and Klein, D. A. (2005) Microbiology 6th Ed. McGraw-Hill Higher Education: Dubuque, IA.

(2) Errington, J. (2003) Regulation of endospore formation in *Bacillus subtilis*. Nature Reviews Microbiology. 1, 117-126. (License # 3272790038340)

(3) MicrobeWiki. Endospore structure. Accessed: 11/19/13.

(4) Setlow, P. (2005) Spores of *Bacillus subtilis:* their resistance to and killing by radiation, heat and chemicals. Journal of Applied Microbiology. 101, 514-525.

(5) Takamatsu, H., and Watabe, K. (2002) Assembly and genetics of spore protective structures. Cellular and Molecular Life Sciences. 59, 434-444.

(6) Lu, X-J., Olson, and W.K. (2013) 3DNA: a software package for the analysis rebuilding and visualization of three-dimensional nucleic acid structures. 31(17) (License # 3252650189403)

(7) Cornell University College of Agriculture and Life Sciences. Department of Microbiology. Accessed 11/4/2013 http://micro.cornell.edu/research/epulopiscium/bacterial-endospores.

(8) Lamola, A. A. (1970) Triplet photosensitization and the photobiology of thymine dimers in DNA. Pure and Applied Chemistry. 24, 599-610.

(9) Cadet, J., and Vigny, P. (1990) Photochemistry and the nucleic acids Vol.1. Wiley: New York.

(10) Durbeej, B., and Eriksson, L. A., (2003) On the formation of cyclobutane pyrimidine dimers in UV-irradiated DNA: Why are thymines more reactive? Photochemistry and Photobiology. 78, 159-167.

(11) Nelson, D.L., Cox, M.M. (2008) Principles of Biochemistry. 5th. Ed. W.H.Freeman and Company. New York, NY.

(12) Lee, K. S., Bumbaca, D., Kosman, J., Setlow, P., and Jedrzejas, M. J. (2008) Structure of a protein-DNA complex essential for DNA protection in spores of *Bacillus* species. Proceedings of the National Academy of Sciences of the United States of America. 105, 2806-2811.

(13) Bumbaca, D., Kosman, J., Setlow, P., Henderson, R. K., and Jedrzejas, M. J. (2007) Crystallization and preliminary X-ray analysis of the complex between a *Bacillus subtilis* [alpha]/[beta]-type small acid-soluble spore protein and DNA. Acta Crystallographica. Section F, Structural Biology and Crystallization Communications. 63, 503-506.

(14) Mohr, S. C., Sokolov, N. V., He, C. M., and Setlow, P. (1991) Binding of small acid-soluble spore proteins from *Bacillus subtilis* changes the conformation of DNA from B to A. Proceedings of the National Academy of Sciences of the United States of America. 88, 77-81.

(15) Nicholson, W. L., Setlow, B., and Setlow, P. (1991) Ultraviolet irradiation of DNA complexed with alpha/beta-type small acid-soluble proteins from spores of *Bacillus* or *Clostridium* species makes spore photoproduct but not thymine dimers. Proceedings of the National Academy of Sciences of the United States of America. 88, 8288-8292.

(16) Setlow, B., and Setlow, P. (1993) Dipicolinic acid greatly enhances production of spore photoproduct in bacterial spores upon UV irradiation. Applied and Environmental Microbiology. 59, 640-643.

(17) Donnellan, J. E., and Stafford, R. S. (1968) The ultraviolet photochemistry and photobiology of vegetative cells and spores of *Bacillus megaterium*. Biophysical Journal. 8, 17-28.

(18) Setlow, P. (1995) Mechanisms for the prevention of damage to DNA in spores of *Bacillus* species. Annual Review of Microbiology. 49, 29-54.

(19) Mantel, C., Chandor, A., Gasparutto, D., Douki, T., Atta, M., Fontecave, M., Bayle, P. A., Mouesca, J. M., and Bardet, M. (2008) Combined NMR and DFT studies for the absolute configuration elucidation of the spore photoproduct, a UV-induced DNA lesion. Journal of the American Chemical Society. 130, 16978-16984.

(20) Lin, G., and Li, L. (2010) Elucidation of spore-photoproduct formation by isotope labeling. Angewandte Chemie. International Edition in English. 49, 9926–9929.

(21) Yang, L., Lin, G., Liu, D., Dria, K., Tesler, J., and Li, L. (2011) Probing the reaction mechanism of spore photoproduct lyase (SPL) via diastereoselectively labeled dinucleotide SP TpT substrates. Journal of the American Chemical Society. 133, 10434-10447.

(22) Moeller, R., Douki, T., Cadet, J., Stackebrandt, E., Nicholson, W. L., Rettberg, P., Reitz, G., and Horneck, G. (2007) UV-radiation-induced formation of DNA bipyrimidine photoproducts in *Bacillus subtilis* endospores and their repair during germination. International Microbiology. 10, 39-46.

(23) Yang, L., and Li, L. (2013) The enzyme-mediated direct reversal of a dithymine photoproduct in germinating endospores. International Journal of Molecular Sciences. 14(7), 13137-13153.

(24) National Center for Biotechnology Information. Accessed Online 11/10/2013. http://www.ncbi.nlm.nih.gov/.

(25) Desnous, C., Guillaume, D., and Clivio, P. (2010) Spore photoproduct: A key to bacterial eternal life. Chemical Reviews. 110, 1213-1232.

(26) Wikipedia. BLAST page. Accessed online 11/10/2013. http://en.wikipedia.org/wiki/BLAST.

(27) Aravind, L., Anantharaman, V., Balaji, S., Mohan Babu, M., and Iyer, L.M. (2005**)** The many faces of the helix-turn-helix domain: Transcription regulation and beyond. FEMS Microbiology Reviews. 29, 231-262

(28) Wang, T.-C. V., and Rupert, C. S., (1977) Evidence for the monomerization of spore photoproduct to two thymines by the light-independent "spore repair" process in *Bacillus subtilis*. Photochemistry and Photobiology. 25, 123-127.

(29) Rebeil, R., Sun, Y., Chooback, L., Pedraza-Reyes, M., Kinsland, C., Begley, T. P., and Nicholson, W. L. (1998) Spore photoproduct lyase from *Bacillus subtilis* spores is a novel iron-sulfur DNA repair enzyme which shares features with proteins such as class III anaerobic ribonucleotide reductases and pyruvate-formate lyases. Journal of Bacteriology. 180, 4879-4885.

(30) Rebeil, R., and Nicholson, W. L. (2001) The subunit structure and catalytic mechanism of the *Bacillus subtilis* DNA repair enzyme spore photoproduct lyase. Proceedings of the National Academy of Sciences of the United States of America. 98, 9038-9043.

(31) Mehl, R. A., and Begley, T. P. (1999) Mechanistic studies on the repair of a novel DNA photolesion: The spore photoproduct. Organic Letters. 1, 1065-1066.

(32) Cheek, J., and Broderick, J. (2002) Direct H atom abstraction from spore photoproduct C-6 initiates DNA repair in the reaction catalyzed by spore photoproduct lyase: Evidence for a reversibly generated adenosyl radical intermediate. Journal of the American Chemical Society. 124, 2860-2861.

(33) Frey, P., and Magnusson, O. (2003) S-Adenosylmethionine: A wolf in sheep's clothing, or a rich man's adenosylcobalamin? Chemical Reviews. 103, 2129-2148.

(34) Gale, J. M., Nissen, K. A., and Smerdon, M. J. (1987) UV-induced formation of pyrimidine dimers in nucleosome core DNA is strongly modulated with a period of 10.3 bases. Proceedings of the National Academy of Sciences of the United States of America. 84(19): 6644–6648.

(35) Gale, J. M., and Smerdon, M. J. (1990) UV-induced (6-4) photoproducts are distributed differently than cyclobutane dimers in nucleosomes. Photochemistry and Photobiology. 51(4):411-7.

(36) Singer Research Group. Ohio State University Department of Chemistry. Accessed 11/4/2013. http://chemistry.osu.edu/~singer/CPD.html.

(37) Guo, J., Luo, Y., and Himo, F. (2003) DNA repair by spore photoproduct lyase: A density functional theory study. Journal of Physical Chemistry. B. 107, 11188-11192.

(38) Himo, F. (2005) C-C bond formation and cleavage in radical enzymes, a theoretical perspective. Biochimica et Biophysica Acta- Reviews on Bioenergetics. 1707, 24-33.

(39) Fajardo-Cavazos, P., Rebeil, R., and Nicholson, W. (2005) Essential cysteine residues in *Bacillus subtilis* spore photoproduct lyase identified by alanine scanning mutagenesis. Current Microbiology. 51, 331-335.

(40) Chandor-Proust, A., Berteau, O., Douki, T., Gasparutto, D., Ollagnier-De-Choudens, S., Fontecave, M., and Atta, M. (2008) DNA repair and free radicals, new insights into the mechanism of spore photoproduct lyase revealed by a single amino acid substitution. Journal of Biological Chemistry. 283, 36361-36368.

(41) Yang, L., Lin, G., Nelson, R. S., Jian, Y., Telser, J., and Li, L. (2012) Mechanistic studies of the spore photoproduct lyase via a single cysteine mutation. Biochemistry. 51 (36), 7173-88.

(42) Yang, L., Nelson, R. S., Benjdia, A.*, Lin, G., Telser, J., Stoll, S., Schlichting, I., and Li, L. (2013) A radical transfer pathway in the spore photoproduct lyase. Biochemistry. 3041-3050

(43) Buis, J., Cheek, J., Kalliri, E., and Broderick, J. (2006) Characterization of an active spore photoproduct lyase, a DNA repair enzyme in the radical S-adenosylmethionine superfamily. Journal of Biological Chemistry. 281, 25994−26003.

(44) Bradford, M. M. (1976) A rapid and sensitive method for the quantitation of microgram quantities of protein utilizing the principle of protein-dye binding. Analytical Biochemistry. 72, 248−254.

(45) Gill, S. C., and Von Hippel, P. H. (1989) Calculation of protein extinction coefficients from amino acid sequence data. Analytical Biochemistry. 182, 319−326.

(46) Fish, W. W. (1988) Rapid colorimetric micromethod for the quantitation of complexed iron in biological samples. Methods in Enzymology. 158, 357−364.

(47) Beinert, H. (1983) Semi-micro methods for analysis of labile sulfide and of labile sulfide plus sulfane sulfur in unusually stable ironsulfur proteins. Analytical Biochemistry. 131, 373−378.

(48) Benjdia, A., Heil, K., Barends, T. R. M., Carell, T., and Schlichting, I. (2012) Structural insights into recognition and repair of UV-DNA damage by spore photoproduct lyase, a radical SAM enzyme. Nucleic Acids Research. 40(18), 9308-18.

(49) Shiio, Y., and Aebersold, R. (2006) Quantitative proteome analysis using isotope coded affinity tags and mass spectrometry. Nature Protocols. 1, 139−145.

(50) Weerapana, E., Wang, C., Simon, G. M., Richter, F., Khare, S., Dillon, M. B. D., Bachovchin, D. A., Mowen, K., Baker, D., and Cravatt, B. F. (2010) Quantitative reactivity profiling predicts functional cysteines in proteomes. Nature. 468, 790−795.

(51) Carroll, K. S., Gao, H., Chen, H. Y., Leary, J. A., and Bertozzi, C. R. (2005) Investigation of the iron-sulfur cluster in *Mycobacterium tuberculosis* APS reductase: Implications for substrate binding and catalysis. Biochemistry. 44, 14647−14657.

(52) Kennedy, M. C., Spoto, G., Emptage, M. H., and Beinert, H. (1988) The active-site sulfhydryl of aconitase is not required for catalytic activity. Journal of Biological Chemistry. 263, 8190−8193.

(53) Carelli, V., Liberatore, F., Scipione, L., Musio, R., and Sciacovelli, O. (2000) On the structure of intermediate adducts arising from dithionite reduction of pyridinium salts: A novel class of derivatives of the parent sulfinic acid. Tetrahedron Letters. 41, 1235−1240.

(54) Carelli, V., Liberatore, F., Scipione, L., Di Rienzo, B., and Tortorella, S. (2005) Dithionite adducts of pyridinium salts: Regioselectivity of formation and mechanisms of decomposition. Tetrahedron. 61, 10331−10337.

(55) Fox, J. L. (1974) Sodium dithionite reduction of flavin. FEBS Letters. 39, 53−55.

(56) Bumbaca, D., Kosman, J., Setlow, P., Henderson, R. K., and Jedrzejas, M. J. (2007) Crystallization and preliminary X-ray analysis of the complex between a *Bacillus subtilis* α/β-type small acid-soluble spore protein and DNA. Acta Crystallographica. Section F, Structural Biology and Crystallization Communications. 63, 503−506.

(57) Henshaw, T. F., Cheek, J., and Broderick, J. B. (2000) The [4Fe-4S]+ cluster of pyruvate formate-lyase activating enzyme generates the glycyl radical on pyruvate formate-lyase: EPR-detected single turnover. Journal of the American Chemical Society. 122, 8331−8332.

(58) Kulzer, R., Pils, T., Kappl, R., Huttermann, J., and Knappe, J. (1998) Reconstitution and characterization of the polynuclear ironsulfur cluster in pyruvate formate-lyase-activating enzyme: Molecular properties of the holoenzyme form. Journal of Biological Chemistry. 273, 4897−4903.

(59) Stubbe, J., and Van Der Donk, W. A. (1998) Protein radicals in enzyme catalysis. Chemical Reviews. 98, 705−762.

(60) Stubbe, J., Nocera, D. G., Yee, C. S., and Chang, M. C. Y. (2003) Radical initiation in the class I ribonucleotide reductase: Long-range proton-coupled electron transfer? Chemical Reviews. 103, 2167−2201.

(61) Lin, G., and Li, L. (2013) Oxidation and reduction of the 5-(2′-deoxyuridinyl) methyl radical. Angewandte Chemie. International Edition in English. 52, 5594-5598.

(62) Hong, I. S., and Greenberg, M. M. (2005) Efficient DNA interstrand cross-link formation from a nucleotide radical. Journal of the American Chemical Society. 127, 3692−3693.

(63) Ding, H., and Greenberg, M. M. (2007) γ-Radiolysis and hydroxyl radical produce interstrand cross-links in DNA involving thymidine. Chemical Research in Toxicology. 20, 1623−1628.

(64) Ding, H., Majumdar, A., Tolman, J. R., and Greenberg, M. M. (2008) Multinuclear NMR and kinetic analysis of DNA interstrand cross-link formation. Journal of the American Chemical Society. 130, 17981−17987.

(65) Peng, X. H., Pigli, Y. Z., Rice, P. A., and Greenberg, M. M. (2008) Protein binding has a large effect on radical mediated DNA damage. Journal of the American Chemical Society. 130, 12890−12891.

(66) Mees, A., Klar, T., Gnau, P., Hennecke, U., Eker, A. P. M., Carell, T., and Essen, L.-O. (2004) Crystal structure of a photolyase bound to a CPD-like DNA lesion after in situ repair. Science. 306, 1789−1793.

(67) Steenken, S. (1992) Electron-transfer-induced acidity/basicity and reactivity changes of purine and pyrimidine bases. Consequences of redox processes for DNA base pairs. Free Radical Research. 16, 349−379.

(68) Teebor, G. W., Frenkel, K., and Goldstein, M. S. (1984) Ionizing radiation and tritium transmutation both cause formation of 5-hydroxymethyl-2′-deoxyuridine in cellular DNA. Proceedings of the National Academy of Sciences of the United States of America. 81, 318−321.

(69) Jursic, B. S. (1999) Reliability of hybrid density theorysemiempirical approach for evaluation of bond dissociation energies. Journal of the Chemical Society, Perkin Transactions. 2, 369−372.

(70) Blanksby, S. J., and Ellison, G. B. (2003) Bond dissociation energies of organic molecules. Accounts of Chemical Research. 36, 255−263.

(71) Hioe, J., and Zipse, H. (2010) Radicals in enzymatic catalysis: A thermodynamic perspective. Faraday Discussions. 145, 301−313.

(72) Hioe, J., and Zipse, H. (2010) Radical stability and its role in synthesis and catalysis. Organic and Biomolecular Chemistry. 8, 3609−3617.

(73) Cotruvo, J. A., and Stubbe, J. (2011) Class I ribonucleotide reductases: Metallocofactor assembly and repair in vitro and in vivo. Annual Reviews of Biochemistry. 80, 733−767.

(74) Frey, P. A., Hegeman, A. D., and Ruzicka, F. J. (2008) The radical SAM superfamily. Critical Reviews in Biochemistry and Molecular Biology. 43, 63−88.

(75) Northrop, D. B. (1975) Steady-state analysis of kinetic isotope effects in enzymic reactions. Biochemistry. 14, 2644−2651.

(76) Cleland, W. W. (1975) Partition analysis and concept of net rate constants as tools in enzyme kinetics. Biochemistry. 14, 3220−3224.

(77) Li, L., and Marsh, E. N. G. (2006) Deuterium isotope effects in the unusual addition of toluene to fumarate catalyzed by benzylsuccinate synthase. Biochemistry. 45, 13932−13938.

(78) Madhavapeddi, P., and Marsh, E. N. (2001) The role of the active site glutamate in the rearrangement of glutamate to 3-methylaspartate catalyzed by adenosylcobalamin-dependent glutamate mutase. Chemistry and Biology. 8, 1143−1149.

(79) Li, L. (2011) Mechanistic studies of the radical SAM enzyme spore photoproduct lyase (SPL). Biochimica et Biophysica Acta-Proteins and Proteomics. 1824(11), 1264-1277.

(80) Marsh, E. N. G., Patterson, D. P., and Li, L. (2010) Adenosyl radical: Reagent and catalyst in enzyme reactions. Chembiochem. 11, 604−621.

(81) Kilgore, J. L., and Aberhart, D. J. (1991) Lysine 2,3-aminomutase: Role of S-adenosyl-L-methionine in the mechanism: Demonstration of tritium transfer from (2RS,3RS)-[3-3H]lysine to Sadenosyl-L-methionine. Journal of the Chemical Society, Perkin Transactions. 1, 79−84.

(82) Aberhart, D. J. (1988) Studies on the mechanism of lysine 2,3-aminomutase. Journal of the Chemical Society, Perkin Transactions. 1, 343−350.

(83) Yokoyama, K., Numakura, M., Kudo, F., Ohmori, D., and Eguchi, T. (2007) Characterization and mechanistic study of a radical SAM dehydrogenase in the biosynthesis of butirosin. Journal of the American Chemical Society. 129, 15147−15155.

(84) Szu, P.-H., Ruszczycky, M. W., Choi, S.-H., Yan, F., and Liu, H.-W. (2009) Characterization and mechanistic studies of DesII: A radical S-adenosyl-L-methionine enzyme involved in the biosynthesis of TDPD-desosamine. Journal of the American Chemical Society. 131, 14030−14042.

(85) Licht, S., Gerfen, G. J., and Stubbe, J. (1996) Thiyl radicals in ribonucleotide reductases. Science. 271, 477−481.

(86) Cleland, W. W. (2005) The use of isotope effects to determine enzyme mechanisms. Archives of Biochemistry and Biophysics. 433, 2−12

(87) Cleland, W. W. (2006) Enzyme mechanisms from isotope effects. In Isotope effects in chemistry and biology (Kohen, A., and Limbach, H.-H., Eds.) Chapter 37, pp 915−930, Taylor & Francis, Boca Raton, FL.

(88) Fersht, A. (1999) Structure and mechanism in protein science: A guide to enzyme catalysis and protein folding, Chapter 3, pp 103−131, W. H. Freeman and Co., New York.

(89) Werst, M. M., Davoust, C. E., and Hoffman, B. M. (1991) Ligand spin densities in blue copper proteins by Q-band 1H and 14N ENDOR spectroscopy. Journal of the American Chemical Society. 113, 1533−1538.

(90) Belford, R. L., and Nilges, M. J. (1979) Computer simulations of powder spectra. In EPR Symposium, 21st Rocky Mountain Conference, Denver, CO.

(91) Jordan, A., and Reichard, P. (1998) Ribonucleotide reductases. Annual Review of Biochemistry. 67, 71−98.

(92) Yagisawa, S. (1989) Two types of rate-determining step in chemical and biochemical processes. Biochemical Journal. 263, 985−988.

(93) Vey, J. L., and Drennan, C. L. (2011) Structural insights into radical generation by the radical SAM superfamily. Chemical Reviews. 111, 2487−2506.

(94) Rigby, S. E. J., Hynson, R. M. G., Ramsay, R. R., Munro, A. W., and Scrutton, N. S. (2005) A stable tyrosyl radical in monoamine oxidase A. Journal of Biological Chemistry. 280, 4627−4631.

(95) Tsai, A.-L., and Kulmacz, R. J. (2010) Prostaglandin H synthase: Resolved and unresolved mechanistic issues. Archives in Biochemistry and Biophysics. 493, 103−124.

(96) Hioe, J., Savasci, G., Brand, H., and Zipse, H. (2011) The stability of Cα peptide radicals: Why glycyl radical enzymes? Chemistry a European Journal. J. 17, 3781−3789.

(97) Hinckley, G. T., and Frey, P. A. (2006) Cofactor dependence of reduction potentials for $[4Fe\text{-}4S]^{2+/1+}$ in lysine 2,3-aminomutase. Biochemical Journal. 45, 3219−3225.

(98) Cavazos, P. F., Nicholson, W. (1995) Molecular dissection of mutations in the *Bacillus subtilis* spore photoproduct lyase gene which affect repair of spore DNA damage caused by UV radiation. Journal of Bacteriology. 177, 4402-4409.